Mesoscale modeling study of the interactions between aerosols and PBL meteorology during a haze episode in China Jing-Jin-Ji and its near surrounding region: Part 1. aerosol distributions and meteorological features

H. Wang[1,2*], M. Xue[1*], X. Y. Zhang[1], H. L. Liu[1], C .H. Zhou[1], S. C. Tan[3], H. Z. Che[1]，B. Chen[3], T. Li[4]

1 Institute of Atmospheric Composition(IAC), Key Laboratory of Atmospheric Chemistry (LAC) of China Meteorological Administration (CMA),Chinese Academy of Meteorological Sciences (CAMS), Beijing, 100081, China

2 Collaborative Innovation Center on Forecast and Evaluation of Meteorological Disasters, Nanjing University of Information Science & Technology, Nanjing 210044, China

3 State Key Laboratory of Numerical Modeling for Atmospheric Sciences and Geophysical Fluid Dynamics (LASG), Institute of Atmospheric Physics, Chinese Academy of Sciences, Beijing, 100029, China

4 School of Atmospheric Physics, Nanjing University of Information Science & Technology, Nanjing 210044,China

Corresponding author: wangh@cams.cma.gov.cn; xm@cams.cma.gov.cn

Abstract

The urbanized region of Beijing-Tianjin-Hebei and its near surrounding region is becoming China's most polluted area by haze, exceeding even the Yangtze and Pearl river deltas. Aside from pollutant emission, the meteorology of the planetary boundary layer (PBL) is the most important factor affecting haze pollution. Focusing on July 2008, the aerosol optical properties and PBL meteorology features closely related with haze formation were simulated in 3JNS region using an online atmospheric chemical transport model. The relationship between regional PBL meteorology, $PM_{2.5}$, and haze is discussed. Model results accurately simulated the aerosol optical depth (AOD), single scattering albedo (SSA) and asymmetry parameter (ASY), validate by comparison with observations from the MODerate Resolution Imaging Spectroradiometer (MODIS), the China Aerosol Remote Sensing NETwork (CARSNET) and the Aerosol Robotic NETwork (AERONET). Modeled PBL wind speeds showed reasonable agreement with those from the National Centers for Environmental Prediction (NCEP) Reanalysis 2. A monthly mean AOD value as high as 1.2 was found from both model and observations, with a daily mean larger than 2.0 during haze episodes in the 3JNS Region. Modeled and observed SSA values of 0.90–0.96 and ASY values of 0.72–0.74 demonstrated the high scattering characteristic of summer aerosols in this region. PBL wind speeds from modeled and NCEP data both showed a reversing trend of $PM_{2.5}$ variation, illustrating the importance of the "PBL window shadow" on haze formation. Turbulence diffusion and PBL height showed had opposite phases to surface $PM_{2.5}$, indicating that lower PBL height and weaker PBL turbulence diffusion are essential to haze formation. It is noted that homogeneous air pressure does not occur at the surface but at an 850–950 hPa height during the haze episode. The momentum transmitting downward of the cold air from above the PBL to the low PBL and surface lead

to an increase in surface wind speeds and haze dispersal.

1. Introduction

With its rapidly expanding urbanization, and both economic and industrial developments, China is faced with increasing poor air quality and haze pollution. There are three main haze pollution regions in eastern China: the Yangtze River delta, the Pearl River (Zhu Jiang) delta, and Beijing-Tianjin-Hebei (shortened to Jing-Jin-Ji) and its near surroundings region (3JNS). These are all areas of high population, rapid economic growth, urbanization and energy consumption *(Zhang et al., 2004; Chak et al., 2008; Che et al., 2009; Wu et al., 2010)*. The Yangtze River Delta region consists of Shanghai, the urban agglomeration of southeast Jiangsu Province and northeast Zhejiang Province. The Pearl River delta metropolitan area includes Guangzhou, Shenzhen, Dongguan, Zhuhai and other nearby cities. The 3JNS Region includes Beijing (Jing), Tianjin (Jin) and Hebei Province (Ji) and their near surroundings including eastern Shanxi province, western Shandong province and northern Henan province.

Many observational and modelling studies have focused on pollution in the Yangtze River delta *(Zhang et al., 2008; Fu et al., 2008; Yin et al., 2009; Gao et al., 2009; Gao et al., 2011; Wang et al., 2012; Kang et al., 2013)* and Pearl River delta regions around the time of their initial, rapid economic development *(Zheng et al., 2000; Lee et al., 2001; Cao et al., 2004; Wu et al., 2006; Chan et al., 2006; Chak et al., 2008; Huang et al., 2008; Tan et al., 2009; Tan et al., 2011)*. However, the 3JNS region has recently become the most polluted area of the three regions and is now attracting serious concern *(Wang et al., 2006; Chen et al., 2007; Wu et al., 2008; Wei et al, 2010; Liu et al., 2010; Wang et al., 2012; Duan et al., 2012; Wang et al, 2014a, 2014b; Che et al., 2014)*. According to the China Environmental Condition Report by the Ministry of Environmental Protection of The People's Republic of China (MEPPRC), seven of the top ten polluted cities in China in the first six months of 2013 –

Xingtai, Shijiazhuang, Handan, Baoding, Tangshan, Hengshui and Langfang – are located in this region However, haze pollution and air quality studies in this region, especially modeling and simulation studies, are rare *(Wang et al., 2008; Xing et al., 2011)* and inadequate compared to the Yangtze River delta and Pearl River delta regions *(Westerdahl, et al., 2009; Zhang et al., 2009, 2013; Zhang et al., 2011; Quan, et al., 2014; Wang et al., 2014a).*

When haze occurs, local meteorological patterns strongly affect the transport and mixing of gases and aerosols, pollutant loading, spatiotemporal distributions and pollution strength. In particular, the meteorological conditions of the local planetary boundary layer (PBL), *e.g.* wind fields, turbulence diffusion, PBL height and atmospheric circulation patterns, are all key to hazy weather, and dominate whether the haze occurs or not since emissions can remain stable within a defined period in a certain area. A PBL parameterization scheme and describing local PBL meteorological conditions in mesoscale atmospheric chemistry models form the base of $PM_{2.5}$ and haze forecasting. In turn, high particle concentrations suspended in the PBL atmosphere during hazy weather may exert a remarkable influence on local PBL meteorology and circulation patterns by reforming the regional solar and thermal radiative budgets.

Focusing on July 2008 over the 3JNS Region, this paper outlines the methodology for the online calculation of aerosol optical features of different species based on an external mixing scheme, introduced into the atmospheric chemical model GRAPES-CUACE for simulating the aerosol optical features and PBL meteorology condition. The local aerosol optical, meteorological and circulation pattern in the PBL as related to haze are also discussed, with a particular focus on the haze episode of July 7–11, 2008. The relationship between key PBL meteorological factors, $PM_{2.5}$ and the haze episode is analyzed. The impact of aerosols on local PBL is presented in a companion paper (Part II).

2. Model Description

The Chinese Unified Atmospheric Chemistry Environment (CUACE) has been integrated into the mesoscale version of Global/Regional Assimilation and PrEdiction System (GRAPES_Meso) developed by the Chinese Academy of Meteorological Sciences, China Meteorological Administration (CMA), to build an online chemical weather forecasting model, GRAPES-CUACE/haze, focusing especially on haze pollution forecasting in China and East Asia. An aerosol radiative parameterization scheme was incorporated into the GRAPES-CUACE model. The aerosol optical depth (AOD), single scattering albedo and asymmetry factor (ASY) is calculated online using this model. The following sections offer a brief introduction to the model.

2.1 GRAPES_Meso

GRAPES_Meso is a real-time operational weather forecasting model used by the CMA, which includes 3-D meteorological field data assimilation, a fully compressible non-hydrostatic model core and a modularized physics package (*Chen et al., 2003; Zhang and Shen, 2008; Chen et al., 2008; Yang et al., 2007*). The model's time integration discretization uses a semi-implicit and semi-Lagrangian temporal advection scheme. The model's horizontal discretization adopts an Arakawa-C staggered grid arrangement and a central finite-difference scheme with second order accuracy, while the model's vertical discretization adopts a non-hydrostatic approximation scheme. Height-based, terrain-following coordinates are used. The model's vertical discretization adopts the vertically-staggered variable arrangement proposed by Charney–Phillips. The large-scale horizontal and vertical transportation and diffusion processes for all gases and aerosols are processed in the dynamic frame of GRAPES_Meso. The GRAPES_Meso3.3 model was released in July

2013 and was used in the GRAPES-CUACE/haze in this study.

The physical processes principally involve large-scale condensation, cumulus convection, micro-physical precipitation, radiative transfer, land surface and boundary layer processes. Each physical process incorporates the use of several schemes *(Xu et al., 2008)*. The model physics schemes and the related lead references used in this study are summarized and list in Table 1. The PBL scheme is very important for correctly modeling and providing accurate weather forecasts (Vogelezang et al., 1996; Santanello et al., 2005), especially for accurate air pollution forecasts (Cheng et al., 2002; Pleim, 2007b). The PBL is the lower tropospheric layer with its height (PBLH) ranging from several hundred meters to a few kilometers, which is one basic feature to the accurate and realistic modeling. The processes of heat, moisture and momentum exchange between the Earth's surface and the rest of the atmosphere all occur within the PBL. The wind speed near the surface, turbulence diffusion, and stability are also calculated in PBL scheme in air quality model. Among the different definitions of PBL, there are still some general agreements. Richardson number (Ri) is usually used by PBLH calculation. A height at which the local Richardson number exceeds a critical value is used to separate stable from turbulent flow. The Hong and Pan Medium Range Forecast (MRF) PBL scheme (Hong and Pan, 1996) was selected for this study (Table 1). The MRF PBL scheme uses nonlocal closure and rely heavily on Ri to compute PBLH. It define PBLH as the height at which a critical Ri is reached 0.5. All the PBL parameters discussed in the following sections are based upon this PBL scheme.

2.2 CUACE

Components of the atmospheric chemistry model CUACE include an emission inventory and process system; gaseous, physical aerosol and chemistry processes; and related thermodynamic equilibrium modules for processing the transformation between gas and particle matter *(Gong and Zhang, 2008; Wang et al., 2009; 2010)*. The CUACE module tracer consists of 66 gas species and seven species of aerosols, with 12 particle size bins.

2.2.1 Emissions

Based on official information about national emission sources in 2006 *(Cao et al., 2006)*, the detailed high-resolution emission inventories of reactive gases, *i.e.* SO_2, NO_x, CO, NH_3 and VOCs, from emissions over China in 2007 were updated to form the current emission data *(Cao et al., 2010)*. The Sparse Matrix Operator Kernel Emissions system (SMOKE) was used to transform this emission data into hourly gridded data as required by the GRAPES_CUACE model, which includes five aerosols species (black carbon (BC), organic carbon (OC), sulfate, nitrate and fugitive dust particles) and 27 gases including VOCs, NH_3, CO, CO_2, SO_x and NO_x *(An et al., 2013)*.

2.2.2 CUACE/Gas

CUACE/Gas is based on the Regional Acid Deposition Model (RADM) *(Stockwell et al., 1990)*, which consists of 66 gaseous species, including five second-order organic aerosols (SOA); 21 photochemical reactions and 121 gas phase reactions are also involved. Wet and dry deposition processes, simple SOA reactions and a liquid phase chemical balance are also included. The gas to aerosol particle transformation process is described using a thermodynamic equilibrium equation.

2.2.3 CUACE/Aero

There are seven species of aerosol considered in CUACE/Aero: sulfates (SF), soil dust (SD), black carbon (BC), organic carbon (OC), sea salts (SS), nitrates (NI) and ammonium salts (AM). The model divides all the aerosol particles into 12 particle size bins with diameter ranges of 0.01–40.96 μm (excluding AM). CUACE/Aero includes the major aerosol processes in the atmosphere: hygroscopic growth, coagulation, nucleation, condensation, dry deposition and sedimentation, below-cloud scavenging, aerosol activation, aerosol–cloud interactions and chemical transformation of sulfur species *(Gong and Zhang, 2008)*.

2.3 On-line Calculation of Optical Properties of Externally-mixed Aerosols

Aerosol chemical properties and sizes are used to calculate aerosol optical and radiative properties. Each chemical constituent of an aerosol is associated with a set of complex refractive index (CRI) data as a function of wavelength. The CRI data of the seven species of aerosols are derived mainly from the HITRAN 2008 database *(Rothman et al., 2009)*, and the Optical Properties of Aerosols and Clouds database (OPAC) *(Hess et al, 1998)*. Optical model data, accounting for East Asian dust using both theory calculation and composition analysis of aerosol samples collected in the Chinese desert during the international project, “Studies on the Origin and Transport of Aeolian Dust and its Effects on Climate” (ADEC), is used to account for Chinese mineral dust CRI data *(Wang et al., 2004; 2006)*. Based on these CRI data and particle sizes in GRAPES_CUACE, Mie theory is used to calculate the key optical parameters of dry aerosol particles in determining aerosols’ direct radiative effects, *i.e.* the extinction coefficient (Q_e), the SSA and the ASY. The mass extinction coefficient (K_{ext} in $m^2\ g^{-1}$) is calculated according to the following formula:

$$Kext_{m,n}(\lambda) = 3Qe_{m,n}(\lambda)/4r_n\rho_m \tag{1}$$

where n represents the particle bin from size 1 to 12 and r_n is the corresponding effective radius of the n^{th} aerosol size, ρ is the particle mass density of the particular aerosol calculated, and m is the aerosol species, *i.e.*

BC, SF, SD, BC, OC, SS, NI or AM, and λ is the wavelength. Figure 1 shows the K_{ext} (Fig. 1a), SSA (Fig. 1b) and ASY (Fig. 1c) for six radii of the model's 12 dry particle size bins (R_dry) from small to large particles of seven species of aerosol. The red line in Fig. 1 indicates the representative particle size bin for the species of aerosol with the highest concentration in the model. For SD aerosol particles, the size range is relatively large and all particle size bins are used, while for AM aerosol particles, only the particle size bin with a radius of 0.06μm is employed. It can be seen from Fig. 1 that the optical features of dry aerosol particles change with chemical composition, particle size and wavelength. These changes are described in the following study of the aerosol radiative parameterization scheme. The AOD of any of the 12 particle bin sizes for any seven of the aerosol species is calculated using:

$$AOD_{m,n}(\lambda) = \sum_{i=1}^{k} Kext_{m,n}(\lambda) C_{m,n} \Delta z_i \tag{2}$$

where $C_{m,n}$ is the mass concentration of the aerosol, n stands for the n^{th} particle size bin and m indicates the aerosol type, i is the index of vertical layers, K is the total number of layers in the model, and Δz_i is the thickness of the model layer. For hygroscopic aerosols, *i.e.* SF, OC, SS, NI and AM, aerosol sizes of wet particles are calculated as a function of relative humidity (RH) using the Kola equation. A total of 10 RH values, 0%, 45%, 50%, 60%, 70%, 80%, 90%, 95%, 98%, and 99%, are considered in the model. The AOD, SSA and ASY of wet particles are a function of chemical composition, RH, particle size and wavelength, which are described as $AOD_{m,n}(rh, \lambda)$, $SSA_{m,n}(rh, \lambda)$ and $ASY_{m,n}(rh, \lambda)$. Figure 2 shows the typical particle size of the above three optical factors (the red line in Fig.1) for five hygroscopic aerosol species at six different RHs. It can be seen from Fig. 2a that the extinction efficiencies of different aerosol species, and their changing trends along with wavelength and RH, are distinctly diverse. Wet aerosols SSA (Fig. 2b) and ASY (Fig. 2c) also show similar dependencies on RH, particle size and chemical composition. Figure 2 indicates a detailed aerosol radiation parameterization scheme considering particle size, atmospheric RH and the particle chemical aerosol composition is essential to evaluate aerosol radiative feedback. An external mixing scheme is used for the different particle size bins for one aerosol type and for different aerosol species to calculate composite aerosol optical properties for each model grid, according the following formulae:

$$AOD\,(rh,\lambda)=\sum_{m=1}^{7}\sum_{n=1}^{12}AOD_{m,n}(rh,\lambda) \tag{3}$$

$$\mathrm{SSA}(rh,\lambda)=\frac{\sum_{m=1}^{7}\sum_{n=1}^{12}SSA_{m,n}(rh,\lambda)\times AOD(rh,\lambda)_{m,n}}{AOD(rh,\lambda)} \tag{4}$$

$$ASY(rh,\lambda)=\frac{\sum_{m=1}^{7}\sum_{n=1}^{12}AOD_{m,n}(rh,\lambda)\times SSA_{m,n}(rh,\lambda)\times ASY_{m,n}(rh,\lambda)}{\sum_{m=1}^{7}\sum_{n=1}^{12}SSA_{m,n}(rh,\lambda)\times AOD(rh,\lambda)} \tag{5}$$

Composite aerosol optical properties change with particle size bin (*n*) and concentration (C_m); RH forecast according to the GRAPES_CUACE model; and wavelength (λ) according to formulae 1–5.

3. Experiment Design

A simulation experiment was achieved in this study through treating any composite aerosol only as a dynamic tracer: the aerosol’s radiation feedback to its dynamic process was not calculated in this model experiment.

The model run for this study commenced on June 25, 2008 and the simulated results for July 1–31, 2008, serve as the base simulations for this research. The GRAPES_CAUCE3.0 model adopts an alterable horizontal resolution, a time step and a forecasting time. There are 31 model layers ascending vertically from the Earth’s surface to 31km height. For the purposes of this study, the horizontal resolution was set to 0.15°×0.15°, the time step to 100 s and the forecasting time to 72 h. The model domain was set as 90–140°E, 20–55°N. NCEP 1×1° Reanalysis data were used for the model’s initial and 6 h meteorological lateral boundary input fields. The monthly mean values of all tracers from observation data are used for initialization at the very beginning of model run. The initial values of all gases in RADM2 and aerosol concentrations are based on the 24 h forecast made by the previous day’s model run. The simulation results after the first three days' model runs are used in this study for eliminating the model errors from the chemical tracer initialization.

4. Results

4.1 Optical properties of aerosols

AOD is a good parameter for elucidating aerosol column loading in the atmosphere. Aerosol optical properties contributing to AOD, SSA and ASY are the most direct and critical parameters for aerosol direct radiative forcing, radiative heating effects, and feedback to atmospheric circulation (*Wang et al., 2006; Huang et al., 2006, 2009*). AOD data from the Moderate Resolution Imaging Spectroradiometer (MODIS), onboard the Aqua satellite, have been widely used in evaluating and investigating the aerosol burden (*Ichoku et al., 2002; Kahn et al., 2007; Zhang and Reid, 2010*). The daily MODIS AOD by Deep Blue algorithm, which fills in data gaps remaining in the Dark Target-Land aerosol retrieval over bright surfaces (*Hsu et al., 2006*), at 550 nm (MODIS/Aqua Collection 5.1 MYD08_D3 product) with a spatial resolution of

1°×1° is used in this paper to evaluate the modeled AOD.

Figure 3 compares the modeled monthly averaged AOD for July with MODIS Deep Blue AOD at 550 nm. It can be seen from Fig. 3 that both the MODIS and modeled AOD results show that the highest AOD values are in the 3JNS region, reaching 1 for most of this region and even 2. As a general rule, the modeled AOD results seem a little higher than the MODIS AOD data. Considering the uncertainties of MODIS Deep Blue AOD over land (*Remer et al., 2005*), especially in spring and summer time in eastern China (*Yang et al., 2011*), its time-limited scans of China, and the different integrating time of the monthly averaged MODIS and modeled AOD, the resulting consistency of the horizontal distribution, the AOD's central location, and the values of both AOD data sets is both acceptable and reasonable. These results also prove the model's performance in July 2008 in describing aerosol column loading and the extinction effects by the composite atmospheric aerosol in this region.

The ground based observed AOD from the China Aerosol Remote Sensing NETwork (CARSNET) (*Che et al., 2008*) is also employed to evaluate the modeled AOD. CARSNET AODs are retrieved in the 440, 675, 870, and 1020 nm bands using the automatic Cimel sun and sky scanning radiometer (Cimel-318, Cimel Electronique). Taking the data continuity and the locations of the stations into account, the AOD at 440 nm at six surface CRASNET stations are used here. The locations and altitudes of these stations are listed in Table 2. The Beijing, Xianghe and Shangdianzi stations are all located in the Beijing metropolitan region. The Beijing station is located in CMA premises, and was taken as representative of urban Beijing, while the Xianghe and Shangdianzi stations are located in the rural areas around Beijing. The city of Lanzhou is taken as having air pollution conditions typical of western China. The Lanzhou CARSNET station is located in urban Lanzhou; the Semi-Arid Climate and Environment Observatory of Lanzhou University (SACOL) station located in the Lanzhou University campus in Yuzhong, outside the city, represents the rural region of Lanzhou (Huang et al., 2008). The Gucheng station located in Hebei Province represents Beijing’s periphery. Datong is a medium-sized city in Shanxi Province, westward and windward of Beijing. All the stations are located in mideastern China, except for Lanzhou.

Figure 4 shows a comparison between daily averaged CRASNET and modeled AOD data in July, 2008. It can be seen that both the simulated and the observed AOD data congruously indicate two pollution episodes in the 3JNS Region, one from 7 to11 July, 2008, in Beijing, Shangdianzi, Gucheng and Datong, and another from 23 to 29 July, 2008 in Beijing, Shangdianzi and Gucheng. Both modeled and observed AOD data show that the daily averaged AOD values reached 1.5–3 during the episode on 7–11 July, 2008, indicating that the pollution affects not only Beijing and its environs, but also Shanxi Province (i.e. Datong) to the west. The 23–29 July, 2008 pollution episode appears weaker, but lasted longer than the episode on 7–11 July, 2008, and was not observed at the Datong station. The modeled and CARSNET AOD data from 1–31 July, 2008 shows fairly consistent diurnal trends, validating the modeled AOD data at these four stations. In Lanzhou, CARSNET AOD values remained low from 1 to 31 July, 2008, and almost all were <0.5, indicating clear air conditions in this city in July. Modeled AOD values show very similar results with the observed CARSNET data, corroborating the model’s validity for western China. For Longfengshan station in northeastern China, the model’s performance is not as good as for other stations as compared to CARSNET AOD data.

SSA and ASY values also have a substantial impact on aerosol radiative effects and feedback to atmospheric circulation, which help determine the existence of aerosol radiative forcing, *i.e.* the heating or cooling of the atmosphere, and the negative or positive radiative feedback from the haze episode itself. The SSA and ASY observation data set from the Aerosol Robotic Network (AERONET) at the Xianghe and SOCAL stations were used to evaluate the model's performance. Monthly averaged AERONET and modeled SSA and ASY were calculated, together with the SSA and ASY bias for the model (Table 3). It can be seen from Table 3 that observed SSA at the Xianghe station was 0.96, and 0.95 at the SOCAL station; the modeled values were 0.93 and 0.90 for the two stations, respectively. AERONET and modeled SSA data for the two stations consistently indicate a high aerosol scattering ratio in western and eastern China. The SSA bias is −3% at the Xianghe station and −5% at the SOCAL station. The AERONET ASY is 0.74 at the Xianghe station and 0.72 at the SOCAL station, while the modeled values are 0.78 and 0.77, respectively. The ASY bias is +5% at the Xianghe station and +7% at the SOCAL station. The SSA and ASY bias for the model is therefore both reasonable and acceptable, taking the experimental sensitivity of the impact of optical properties on radiative forcing into account *(Wang et al., 2006)*. It is worth noting that both the SSA and ASY observed data sets for the Chinese mainland are sparse. Only 10 days' SSA and ASY data for the Xianghe station, and seven days' SSA data and 17 days' ASY data for the SOCAL station were available for evaluating this study's modeled results.

The vertical distribution of the aerosol layer is the other key factor affecting aerosol radiation besides chemical composition and optical characteristics. Diurnal changes in the vertical distribution of $PM_{2.5}$ for the 3JNS region from 1–31 July, 2008 were calculated and are displayed in Fig. 5a. It can be seen that the $PM_{2.5}$ pollutants were generally concentrated in the surface and near surface atmosphere in July, 2008. A $PM_{2.5}$ concentration >120 μg m^{-3} generally occurs below 800 hPa, overlapping the PBL height, or a little higher. The greatest height of the concentrated $PM_{2.5}$ layer varies between 700 hPa to 900 hPa on different days. Figure 5b shows the vertical distribution of averaged $PM_{2.5}$ and K_{ext} for 7–11 July, 2008. A $PM_{2.5}$

concentration >150 μg m^{-3} occurs below 900 hPa and a concentration of >110 μg m^{-3} is found below 800 hPa. The highest K_{ext} value appears at 800 hPa, suggesting that the greatest aerosol extinction occurs in the upper PBL, or above it, aiding the cooling of the lower PBL and the heating of the upper PBL.

4.2 PBL meteorological features corresponding to the haze episode

The PBL wind speed, diffusion coefficient and PBL height are the most important parameters representing the PBL characteristics affecting air and haze pollution. The terms “window shadow”, “homogeneous air pressure” and “stable and steady” have been used to describe the typical patterns of local air circulation and surface meteorological fields for haze episodes. In the following section, these three factors and their correlation with particulate $PM_{2.5}$ pollutants are discussed. Air pressure patterns are also used to discuss the strength of, and changes in, PBL cold air; these patterns have an important effect on air pollution episodes, and most especially upon the weakening and collapsing of haze episodes.

4.2.1 Planetary boundary layer winds

Not only do the surface winds directly impact haze impacts, but also the winds in the whole PBL. The accuracy of the model’s forecasting of surface and PBL winds is critical for an accurate haze prediction. The conventional meteorology observation data from sounding balloons are only available at 00:00 and 12:00 UTC in China (early morning or dust in local time). The NCEP/NCAR Reanalysis-2 meteorology data are available for numerous meteorological parameters including geopotential height, air temperature, vertical velocity, wind field, etc., at a time resolution of 6 hours (00:00, 06:00, 12:00, and 18:00 UTC) at sea level pressure, 1000, 950, 850, 700, 500, 300 hPa, etc. heights. In view of the importance of daytime PBL meteorology conditions to haze episode, Reanalysis-2 data are used to evaluate the model's results and study the PBL features instead of sounding balloon observations, due to the lack of daytime PBL meteorology data from the latter.

Figure 6 shows the model's daily averaged wind speeds and the NCEP analysis for the 3JNS Region for 1–31 July, 2008, together with $PM_{2.5}$ at the surface (Fig. 6a) and at 850–950 hPa (Fig. 6b). It can be seen that the modeled wind speed at 850–950 hPa agrees well with the NCEP wind speed, showing the model's fair ability to predict wind speed at this height. Averaged modeled $PM_{2.5}$ for the same region at 850–950 hPa is also shown in Fig. 6a. It can be seen that the diurnal variations in $PM_{2.5}$ in the PBL evince a completely contrary phase, shifting with the wind speeds of both modeled and NCEP Reanalysis, *i.e.* the peak values of $PM_{2.5}$ correspond with the trough values of wind speed, showing that low wind speed in the PBL may be the most important factor leading to haze pollution. Modeled surface wind values also correspond fundamentally with NCEP data, though not at 850–950 hPa. Nonetheless, the modeled surface wind speed and $PM_{2.5}$ show opposing trends, similar with the 850–950 hPa findings. Corresponding wind speeds are as low as 0.5 m s^{-1} at the surface and are <2m s^{-1}, rising to 4–5m s^{-1} at 850–950 hPa separately during the severe haze pollution episodes of 7–11 and 25–28 July, 2008.

4.2.2 Planetary boundary layer turbulence diffusion

Turbulence diffusion is another important process significantly affecting surface pollutant concentration, since it defines horizontal transportation distance by affecting the vertical heights that pollutants may reach. The turbulence diffusion coefficient (*fktm*) parameterizes the PBL turbulence diffusion process *(Wang et al., 2010)*. Figure 7 shows the averaged surface $PM_{2.5}$ and f_{ktm} horizontal distribution for 7–11 July, 2008 (Fig. 7a), together with the diurnal changes of the 3JNS averaged $PM_{2.5}$ and f_{ktm} (Fig. 7b) from 1 to 31 July, 2008. Figure 7a shows that lower f_{ktm} and higher $PM_{2.5}$ values occurred throughout mid- and eastern China during 7–11 July, 2008. The lowest f_{ktm} values and highest 400 $PM_{2.5}$ values appeared in the 3JNS region, showing the importance of turbulence diffusion on the strength of severe air pollution. It also can be seen from Fig. 7a that $PM_{2.5}$ concentrations exhibit higher values when f_{ktm} are lower, and that this is more marked over the 3JNS region than over southeastern China (22–30°N, 110–120°E). The daily averaged f_{ktm} and $PM_{2.5}$ values for the 3JNS region (Fig. 7b) show a marked correlation over the severely polluted parts of this region. There is a basic reverse trend in daily f_{ktm} and $PM_{2.5}$ values.

4.2.3 Planetary boundary layer height

PBL height is one of the most important variables in any PBL scheme. PBL height can be variously defined by reference to the local Richardson number, the height of the capping inversion, the proportionality of PBL height to the ratio between the friction velocity and the local Coriolis force parameter, the height of the minimum sensible heat flux, turbulent kinetic energy, or a specific vertical potential temperature gradient *(Cheng et al., 2002; Santanello, et al., 2005; Hong et al., 2006; Pleim et al., 2007b)*. Despite all these different definitions, some commonality of agreement on the definition of PBL height exists, *e.g.* the Richardson number, the capping inversion or the height where the potential temperature lapse rate becomes too positive, and so on. The medium-range forecast (MRF) PBL scheme uses non-local closure and relies heavily on Richard index (*Ri*) to compute the PBL height for different regimes (*Hong and Pan, 1996*).

Figure 8 shows the horizontal distribution of the averaged surface $PM_{2.5}$ and PBL height for 7–11 July, 2008 (Fig. 8a), together with diurnal regional trends in the 3JNS averaged $PM_{2.5}$ and PBL height (Fig. 8b). The PBL height values (Fig. 8a) are as low as 300–900 m with high $PM_{2.5}$ values over eastern China, consistent with observational studies of this region *(Wang et al., 2012)*.

The lowest PBL height almost overlaps with the regions of lowest f_{ktm} and highest $PM_{2.5}$ over mideastern China for this period. Comparing the similarly economically developed areas of mideastern and southeastern China (22–30°N, 110–120°E), mideastern China is much more severely polluted. This would suggest that a lower PBL height and weak turbulence diffusion (Fig. 7a) may be two of the main factors leading to higher pollution over this area. Diurnal changes in averaged PBL height and $PM_{2.5}$ over the central polluted area (Fig. 8b) also display a generally contrary correlation during July 2008, indicating the important impact of the PBL height on the pollution strength (PM2.5 concentration) of the surface air, *i.e.* low PBL height and f_{ktm} are critical to the degree of haze pollution.

4.2.4 Patterns in planetary boundary layer air pressure fields

Surface “homogeneous air pressure” has been regarded as a typical surface air pressure feature associated with haze pollution *(Liu et al., 2010)*. Detailed comparisons of PBL air pressure patterns between hazy and clear conditions for different seasons are, at present, limited. Modeled $PM_{2.5}$, AOD and CARSNET AOD data (Fig. 4) all show that July 10, 2008, was the severest haze day, while July 12, 2008, was the first clear day after this haze episode. Figure 9 displays the air pressure pattern, wind speed vector at the surface (bottom), geopotential height and wind speed vector at 950 hPa (middle) and 850 hPa (top) on 10 July, 2008 (left), and 12 July, 2008 (right). July is midsummer in China and a subtropical high with high pressure contolled the surface in eastern China and the sea region east of China on 10 July, 2008. No obvious difference was observed between the surface air pressure pattern on 12 July, 2008 and on 10 July, 2008 due to the effect of the strong subtropical high to the east. The patterns of geopotential heights for 850–950 hPa heights are quite different from those for surface pressure, showing a “homogeneous air pressure pattern” over the whole of eastern China on 10 July, 2008. The southeasterly weakening and retrenchment of the subtropical high from 10 to 12 July, 2008 is clear at 850–950 hPa height. The main area of subtropical high pressure withdrew across the sea west of the Korean Peninsula on 12, 2008. At the same time, cold air from Mongolia moved to midnorthern China, and the air pressure over this region strengthened at 850–950 hPa during 10–12 July, 2008. Eastern China was controlled by continental high pressure from the northwest, increasing the northerly wind speed over mideastern China at 850–950 hPa on 12 July, 2008. The surface wind vector shows that over mideastern China, the northerly wind speed on 12 July, 2008, was obviously higher than that on 10 July, 2008. This was not caused by any pressure-gradient force because the air pressure patterns on 10 and 12 July, 2008, were very similar, but the transfer of cold air and momentum from 850–950 hPa to the surface led to an increase in the northerly wind speed at the surface, directly bringing the haze episode to an end over the mid- and eastern China including the 3JNS Region.

5. Conclusion

The mesoscale chemical weather forecasting model GRAPES-CUACE/haze, integrated with an online radiative parameterization scheme, based on an external mixing scheme of black carbon, organic carbon, soil dust, nitrates, sulfate, sea salt and ammonia aerosols, was employed to simulate the optical characteristics of aerosols and the PBL meteorological features related to haze in July 2008. The aerosols' AOD, SSA and ASY features were simulated and evaluated. The PBL characteristics of aerosol loading, PBL heights, turbulence diffusion, wind speed, air pressure, geopotential height patterns and their relation to haze and $PM_{2.5}$ were evaluated and the results are summarized below.

The comparison between modeled AOD, SSA, and ASY data and MODIS, CARSNET and AERONET observational data confirms the model's ability to predict aerosol column loading and aerosol optical features, fundamental to studying and evaluating the aerosols' radiative feedback to regional and local PBL circulation. The modeled PBL wind speed correlates closely with the NCEP analysis data, showing the model's ability to predict PBL wind speeds as a base for haze forecasting. Modeled and observed AOD showed that the monthly mean AOD values may exceed 1.2 and the daily mean value was likely larger than 2.0 for the period 7–11 July, 2008 in the 3JNS Region. SSA is as high as 0.90–0.96 and ASY is 0.72–0.74, showing the high scattering properties of aerosols in summer. The PBL wind speed from modeled and NCEP Reanalysis data both show a completely inverse trend with $PM_{2.5}$, changing diurnally. This illustrates the importance of the "PBL window shadow" to the haze episode. Low turbulence diffusion and PBL height are also important meteorological factors affecting haze episodes, as evident from their correlation with near-surface $PM_{2.5}$ either on a regional or a diurnal basis.

Contrary to the findings of most previous studies, a "homogeneous air pressure pattern" appears not to be typical of the surface pressure field in summer in middle and eastern China: surface pressure patterns are almost identical for both a hazy day (July 10, 2008) and a clear day (12 July, 2008) after haze. The geopotential height patterns of the PBL (850–950 hPa) show a "homogeneous air pressure" field in middle and eastern China between the land-based, cold high over northwest China and Mongolia and the subtropical high over the East China Sea on a hazy day (10 July, 2008). The haze ended on 12 July, 2008 over eastern China, accompanied by an extension into midnorthern China of the land-based cold high from the northwest, and a weakening and easterly retrenchment to the east of the subtropical high. The PBL "homogeneous air pressure" over middle and eastern China was disrupted and cold air from Mongolia controlled midnorthern China at 850–950 hPa. This resulted in the wind speed increasing in middle and eastern China at this height. A downward momentum from the PBL (850–950 hPa) to the surface directly led to the surface wind increasing, and, combined with the PBL cold air, this resulted in the collapse of the hazy weather over eastern China.

Since all discussions above are based on the results from a haze episode in July 2008, any conclusions drawn concerning PBL meteorological and aerosol optical features during hazy weather may only apply to summer haze episodes. Haze episodes in other seasons need to be studied: the results may be different because of the different prevalent meteorological conditions in different seasons. In this study, aerosol optical parameters were calculated online, but their radiative effects were not entered online to the model's dynamical process. In the companion paper, aerosol radiative feedback and its impact on PBL meteorology and the haze episode itself will be implemented and discussed in detail.

Acknowledgments

This work is supported by the National Basic Research Program (973) (Grant Nos. 2011CB403404), the National Natural Scientific Foundation of China (Grant Nos. 41275007, 41130104, and 41475136), and CAMS Key Projects (Grant No. 2013Z007).

References

An, X. Q., Sun, Z. B., Lin, W. I., Jin, M., and Li, N.: Emission inventory evaluation using observations of regional atmospheric background stations of China, J. Environ. Sci., 25 (3), 537–546, 2013.

Chak K. C., and Yao, X. h.: Review Air pollution in mega cities in China, Atmos. Environ., 42, 1–42, 2008.

Cao, J. J., Lee, S. C., Ho, K. F., Zou, S. C., Fung, K., Li, Y., Watson, J. G., and Chow, J. C.: Spatial and seasonal variations of atmospheric organic carbon and elemental carbon in Pearl River Delta Region, Chin. Atmos. Environ., 38, 4447–4456, 2004.

Cao, G., Zhang, X., and Zheng, F.: Inventory of black carbon and organic carbon 446 emissions from China, Atmos. Environ., 40, 6516–27, 2006.

Cao, G. L.， AN, X. Q., Zhou C. H., Ren, Y. Q., and Tu, J.: Emission inventory of air pollutants in China, Chin. Environ., Sci., 30 (7),900~906, 2010.

Chan, C. Y., Tang, J. H., Li, Y. S., and Chan, L. Y.: Mixing ratios and sources of halocarbons in urban, semi-urban and rural sites of the Pearl River Delta, South China, Atmos. Environ., 40, 7331–7345, 2006.

Che, H., Zhang, X., Chen, H., Damiri, B., Goloub, P., Li, Z., Zhang, X., Wei, Y., Zhou, H., Dong, F., Li, D., and Zhou, T.: Instrument calibration and Aerosol Optical Depth (AOD) validation of the China Aerosol Remote Sensing Network (CARSNET), J. Geophys. Res., 114. doi:10.1029/2008JD011030, 2008.

Che, H. Z., Zhang, X. Y., and Li, Y.: Haze trends over the capital cities of 31 provinces in China, 1981-2005, Theor. App. Clim., 97, 235-242, 2009.

Che, H., Xia, X., Zhu, J., Li, Z., Dubovik, O., Holben, B., Goloub, P., Chen, H., Estelles, V., Cuevas-Agulló, E., Blarel, L., Wang, H., Zhao, H., Zhang, X., Wang, Y., Sun, J., Tao, R., Zhang, X., and Shi, G.: Column aerosol optical properties and aerosol radiative forcing during a serious haze-fog month over North China Plain in 2013 based on ground-based sunphotometer measurements, Atmos. Chem. Phys., 14, 2125-2138, doi:10.5194/acp-14-2125-2014, 2014.

Chen, D. H., Xue, J. S., and Yang, X. S.: The new generation of hydrostatic/nonhydrostatic multi-scales numerical prediction model: Scientific design and experiments (in Chinese), CAMS Technical Report 1., 2003.

Chen, D. H, Xue, J. S., Yang, X. S., Zhang, H. L., Shen, X. S., Hu, J. L., Wang, Y., Ji , L. R., Chen, J. B.: (New generation of multi-scale NWP system (GRAPES): general scientific design, Chin. Sci. Bull., 53(22), 3433-3445, 2008.

Chen, Z. H., Cheng, S. Y., and Su, F. Q.: Analysis of large-scale weather pattern during heavy air pollution process in Beijing), Res. Environ. Sci. (in Chinese), 20 (2), 99-105, 2007.

Cheng, Y., Canuto, V. M., and Howard, A. M.: An improved model for the turbulent PBL, J. Atmos. Sci., 59, 1550–1565, 2002.

Chou, M. D., Suarez, M. J., Ho, C. H., Yan, M. M. H., and Lee, K. T.: Parameterizations for Cloud Overlapping and Shortwave Single-Scattering Properties for Use in General Circulation and Cloud Ensemble Models, J. Clim., 11, 202–214, 1998.

Chou, M. D., Suarez, M. J., Liang, X. Z., and Michael M.-H. Y.: A Thermal Infrared Radiation Parameterization for Atmospheric Studies, Technical Report Series on Global Modeling and Data Assimilation, NASA/TM-2001-104606, 19, America, Goddard Space Flight Center, Greenbelt, Maryland, 55, 2001.

Duan, J. C., Guo, S. J., Tan, J. H., Wang, S., and Chai, F. H. : a Characteristics of atmospheric carbonyls during haze days in Beijing, China, Atmos. Res., 114-115, 17-27, 2012.

Fu, Q. Y., Zhuang, G. S., Wang, J., Xu, C., Huang, K., Li, J., Hou, B., Lu, T., and Streets, D. G.: Mechanism of formation of the heaviest pollution episode ever recorded in the Yangtze RiverDelta, China, Atmos. Environ. 42, 2023–2036, 2008.

Gao, J., Wang, T., Zhou, X. H., Wu, W. S., and Wang, W. X.: Measurement of aerosol number size distributions in the Yangtze River delta in China: formation and growth of particles under polluted conditions, Atmos. Environ., 43, 829–836, 2009.

Gao, L. N., Jia, G. S., Zhang, R. J., Che, H. Z., Fu, C. B., Wang, T. J., Zhang, M. G., and Jiang, H.: Visibility trends in the Yangtze River Delta of China during 1981-2005, J. Air. Waste. Manage., 61, 843-849, 2011.

Gong, S. L, and Zhang, X. Y.: CUACE/Dust – an integrated system of observation and modeling systems for operational dust forecasting in Asia, Atmos. Chem. Phys., 8, 2,333-82,340, 2008.

Hess, M., Koepke, P., and Schult, I., Optical Properties of Aerosols and Clouds: The software package OPAC, Bull. Am. Met. Soc., 79, 831-844, 1998.

Hong, S. Y. and Pan, H. L.: Nonlocal boundary layer vertical diffusion in a Medium-Range Forecast model, Mon. Weather Rev., 124, 2322–2339, 1996.

Hong, S. Y., Noh, Y., and Dudhia, J.: A new vertical diffusion package with an explicit treatment of entrainment processes, Mon. Wea. Rev., 134, 2318–2341, 2006.

Huang, J., Lin, B., Minnis, P., Wang, T., Wang, X., Hu, Y., Yi, Y., and Ayers, J.: Satellite-based assessment of possible dust aerosols semi-direct effect on cloud water path over East Asia, Geo. Res. Let., 33 (19), L19802, doi:10.1029/2006GL026561, 2006.

Huang, J. P., Zhang, W., Zuo, J. Q., Bi, J. R., Shi, J. S., Wang, X., Chang, Z. L., Huang, Z. W., Yang, S., Zhang, B. D., Wang, G. Y., Feng, G. H., Yuan, J. Y., Zhang, L., Zuo, H. C., Wang, S. G., Fu, C. B., and Chou, J. F. : An overview of the semi-arid climate and environment research observatory over the Loess Plateau. Adv. Atmos. Sci., 25(6), 906–921, 2008.Huang, J., Wu, D., Huang, M. H., Li, F., Bi, X. Y., Tan, H. B., and Deng, X. J.: Visibility variations in the Pearl River delta of China during the period of 1954–2004, J. App. Meteor., 19, 61–70, 2008.

Huang, J., Fu, Q., Su, J., Tang, Q., Minnis, Y., Hu, P., Yi, Y., and Zhao, Q.: Taklimakan dust aerosol radiative heating derived from CALIPSO observations using the Fu-Liou radiation model with CERES constraints, Atmos. Chem. Phys., 9 (12), 2009.

Hsu, N. C., Si-Chee, T., King, M. D., and Herman, J. R., : Deep Blue Retrievals of Asian Aerosol Properties During ACE-Asia, Geoscience and Remote Sensing, IEEE Transactions on, 44(11), 3180-3195, 2006.

Ichoku, C., Chu, D.A., Mattoo, S., Kaufman, Y.J., Remer, L.A., Tanré, D., Slutsker, I., and Holben, B.N.: A spatio-temporal approach for global validation and analysis of MODIS aerosol products, Geophys. Res. Let., 29 (12), 8006. doi:10.1029/2001GL013206, 2002.

Kang H. Q., Zhu, B., Su, J. F., Wang, H. L., Zhang, Q. C., and Wang, F. : Analysis of a long-lasting haze episode in Nanjing, China, Atmos. Res., 78-87, 2013.

Kahn, R., Garay, M., Nelson, D., Yau, K., Bull, M., and Martonchik, J.: Satellitederived aerosol optical depth over dark water from MISR and MODIS: comparisons with AERONET and implications for climatological studies. J. Geophys. Res., 112, D18205, doi:10.1029/2006JD008175, 2007.

Kessler, E.: On the distribution and continuity of water substance in atmospheric circulation, Meteor. Monogr., 32, Amer. Meteor. Soc., 84pp, 1969.

Kain, J. S.: The Kain-Fritsch convective parameterization: An update, J. Appl. Meteor., 43, 170–181, 2004.

Kusaka, H., Kondo, H., Kikegawa, Y., Kimura, F.: A simple single-layer urban canopy model for atmospheric models: Comparison with multi-layer and slab models. Bound.-Layer Meteor., 101, 329–358, 2001.

Lee,Y. L., and Sequeira, R.: Visibility degradation across Hong Kong: its components and their relative contributions, Atmos. Environ., 34, 5861–5872, 2001.

Liu, X. H., Zhang, Y., Cheng, S. H., Xing, J., Zhang, Q., Streets, D. G., Jang, C., Wang, W. X., and Hao, J. M.: Understanding of regional air pollution over China using CMAQ, part I performance evaluation and seasonal variation, Atmos. Environ., 44, 2415-2426, 2010.

Liu W. D., Jiang, Y. H., and Li, J.: Characteristics of aerosol distribution and transmission of a heavy air pollution process in Beijing area, Clim. Environ. Res. (in Chinese), 15 (2), 152- 160, 2010.

Pleim, J. : A combined local and non-local closure model for the atmospheric boundary layer. Part II: Application and evaluation in a mesoscale meteorological model, J. Applied Meteor. Climatology, 46, 1396–1409, 2007.

Quan. J., Tie, X., Zhang., Q., and Liu, Q.: Characteristics of heavy pollution during the 2012-2013 winter in Beijing, China. Atmos. Envoirn., 88, 83-89, 2014.

Rothman, L.S., Gordon, I.E., Barbe, A., Chris Benner, D., ,Bernath, P.F., Birk, M., ,Boudon, V., Brown, L.R., Campargue, A., Champion, J.P., Chance, K., Coudert, L.H., Dana, V., ,Devi, V.M., Fally, S., Flaud, J.-M., Gamache, R.R., Goldman, A., Jacquemart, D., Kleiner, I., Lacome, N., Lafferty, W.J., Mandin, J.-Y., ,Massie, S.T., Mikhailenko, S.N., Miller, C.E., Moazzen-Ahmadi, N., Naumenko, O.V., Nikitin, A.V., Orphal, J., Perevalov, V.I., Perrin, A., Predoi-Cross, A., Rinsland, C.P., Rotger, M., Šimečková, M., Smith, M.A.H., Sung, K., Tashkun, S.A., Tennyson, J., Toth, R.A., Vandaele, A.C. and Vander Auwera, J.: The HITRAN 2008 molecular spectroscopic database, J. Quant. Spect. and Rad. Trans., 110 (9-10), 533-572, 2009.

Remer, L. A., Kaufman, Y. J., Tanre, D., Mattoo, S., Chu, D. A., Martins, J. V., Li, R. R., Ichoku, C., Levy, R. C., Kleidman, R. G., Eck, T. F., Vermote, E., Holben, B. N.: The MODIS Aerosol Algorithm, Products, and Validation, J. Atmos. Sci., 66, 947-973, 2005.

Santanello, J. A., Friedl, M. A., and Kustas, W. P. : An empirical investigation of convective planetary boundary layer evolution and its relationship with the land surface, J. Applied Meteor., 44, 917–932, 2005.

Stockwell, W. R., Middleton, P., Chang, J. S., Tang X.: The Second Generation Regional Acid Deposition Model Chemical Mechanism for Regional Air Quality Modeling, J. Geophys. Res. 95, 16343- 16376,1990.

Tan, J., Duan, J., Chen, D., Wang, X., Guo, S., Bi, X., Sheng, G., He, K., and Fu, J. : Chemical characteristics of haze during summer and winter in Guangzhou, Atmos. Res., 94, 238-245, 2009.

Tan, J., Guo, S. J., Ma, Y. L., Duan, J. C., Cheng., Y., He., K. B., and Yang, F. M.: Characteristics of particulate PAHs during a typical haze episode in Guangzhou, China, Atmos. Res., 102, 91-98, 2011.

Vogelezang, D. H. P., and Holtslag, A. A. M. : Evaluation and model impacts of alternative boundary-layer height formulations, Bound. Layer Meteor., 81, 245-269, doi:10.1007/BF02430331, 1996.

Wang, L. T., Hao, J. M., and He, K. B.: A modeling study of coarse particulate matter pollution in Beijing: regional source contributions and control implications for the 2008 Summer Olympics, J. Air. Waste. Mnanage., 58, 1057e1069. doi:10.3155/1047-3289.58.8.1057, 2008.

Wang, L. T., Xu, J., Yang, J., Zhao, X. J., Wei, W., Cheng, D. D., Pan, X. M., and Su, J.: Understanding haze pollution over the southern Hebei area of China using the CMAQ model, Atmos. Environ., 56, 69-79, 2012.

Wang, H., Shi, G. Y., Aoki, T., Wang, B., and Zhao, T. L.: Radiative forcing due to dust aerosol over east Asia-north Pacific region during spring 2001， Chin. Sci. Bull., 49(20), 2212-2219, 2004.

Wang, H., Shi, G. Y., Li., W., and Wang, B.: The impacts of optical properties on radiative forcing due to dust aerosol, Adv. Atmos. Sci., 23（2），431- 441, 2006.

Wang, H., Gong, S. L., Zhang, H. L., Chen, Y., Shen, X. S., Chen, D. H., Xue, J. S., Shen, Y. F., Wu, X. J., and Jin, Z. Y.: A new-generation sand and dust storm forecasting system GRAPES_CUACE/Dust: Model development, verification and numerical simulation. Chin. Sci. Bull, doi:

10.1007/s11434-009-0481-z, 2009.

Wang, H., Zhang, X. Y., Gong, S., Chen, Y., Shi, G., and Li, W.: Radiative feedback of dust aerosols on the East Asian dust storms, J. Geophys. Res., 115, D23214, doi:10.1029/2009JD013430, 2010.

Wang H., Tan, S. C., Wang, Y., Jiang, C., Shi, G. Y., Zhang M., Che, H. Z.: A multisource observation study of the severe prolonged regional haze episode over eastern China in January 2013. Atmos. Environ., 89, 807-815, 2014a.

Wang, H., Xu, J. Y., Zhang, M., Yang, Y. Q., Shen, X., J., Wang, Y. Q., Chen, D., Guo, J. P.: A study of the meteorological causes of a prolonged and severe haze episode in January 2013 over central-eastern China, Atmos. Environ., 98, 146-157, 2014b.

Wang, T. J., Jiang, F., Deng, J. J., Shen, Y., Q., Fu, Y., Wang, Q., Fu, Y., Xu, J. H.: Urban air quality and regional haze weather forecast for Yangtze River Delta region, Atmos. Environ., 58, 70-83, 2012.

Wang, Y., Zhuang, G., Sun, Y., and An, Z. : The variation of characteristics and formation mechanisms of aerosols in dust, haze, and clear days in Beijing, Atmos. Environ., 40, 6579 – 6591, 2006.

Wang, Y. T., Li, W.，Zhang X. L., and Meng, W.: Relationship between atmospheric boundary layer and air pollution in summer stable weather in the Beijing urban area［J］. Res. Environ. Sci.，25 (10),1092-1098, 2012.

Wei, W. X., Zhang, X., and Tian, G. Q.: Analysis of relation between haze distribution and terrain and wind speed in Hebei Province, J. Nat. Disasters (in Chinese), 19 (1), 49-52, 2010.

Westerdahl, D., Wang, X., Pan, X., and Zhang, K. M.: Characterization of on-road vehicle emission factors and microenvironmental air quality in Beijing, China. Atmos. Environ., 43(3), 697-705, 2009.

Wu, Z. J., Hu, M., Lin, P., Liu, S., Wehner, B., and Wiedensohler, A. : Particle number size distribution in the urban atmosphere of Beijing, China. Atmos. Environ. 42, 7967–7980, 2008.

Wu, D., Tie, X. X., Li, C. C., Ying, Z. M., Lau, A. K., Huang, J., Deng, X. J., Bi, X. Y. : An extremely low visibility event over the Guangzhou region: a case study, Atmos. Environ., 39, 6568–6577, 2006.

Wu, D., Wu, X. J., and Li, F.: Temporal and spatial variation of haze during 1951-2005 in Chinese mainland, Acta. Meteor. Sinica. (in Chinese), 68, 680-688, 2010.

Xing, J., Zhang, Y., and Wang, S. X. : Modeling study on the air quality impacts from emission reductions and a typical meteorological conditions during the 2008 Beijing Olympics, Atmos. Environ., 45, 1786-1798, 2011.

Xu, G. Q, Chen, D. H, and Xue, J.S.: The program structure designing and optimizing tests of GRAPES physics, Chin Sci Bull, 2008, 53(22), 3470-3476, 2008.

Yang, S., Guang, Y. S., Chen, L., Wang, B., Yang, H. L.: Evaluation of Moderate-Resolution Imaging Spectroradiometer (MODIS) Deep Blue Aerosol Products Using Ground-Based Measurements over Beijing, SOLA, 7, 133−136, doi:10.2151/sola.2011-034, 2011.

Yang, X. S., Chen, J. B., and Hu, J. L.: A semi-implicit semi-Lagran global nonhydrostatic model and the polar discretization scheme, Sci. China Ser D-Earth Sci., 2007, 50(2),1885-1891, 2007.

Yin, Y., Tong, Y. Q., Wei, Y. X., Wang, T. J., Li, J. P., Yang, W. F., and Fan, S. X.: The analysis of chemistry composition of fine-mode particles in Nanjing, Trans, Atmos. Sci., 32 (6), 723–733 (in Chinese), 2009.

Zhang, M., Uno, I., and Yoshi, Y.: Transport and transformation of sulfur compounds over East Asia during the TRACE-P and ACE-Asia campaigns, Atmos. Environ., 38, 6947-6959, 2004.

Zhang, R. H., and Shen, X. S.: On the development of the GRAPES—A new generation of the national operational NWP system in China. Chin. SCI. Bull., 53(22), 3429－3432, 2008.

Zheng, M., and Fang, M.: Particle-associated polycyclic aromatic hydrocarbons in the atmosphere of Hong Kong, Water. Air and Soil

Pollution, 117, 175–189, 2000.

Zhang, J., and Reid, J.S.: A decadal regional and global trend analysis of the aerosol optical depth using a data-assimilation grade over-water MODIS and Level 2MISR aerosol products. Atmos. Chem. Phys, 10, 10949-10963, 2010.

Zhang, X. Y., Wang, Y. Q., and Lin, W. L.: Changes of atmospheric composition and optical properties over Beijing 2008 Olympic monitoring Campaign, BAMS, 1634–1651, 2009.

Zhang, X. Y., Zhang Y. F.，Feng, Y. C., Han, S. Q., Han, B.，LI, L.，XU, H.: Influence of Synoptic Patterns on the Concentrations of PM10 in Tianjin, Res. of Environ. Sci. (in Chinese), 23(9), 1115-1116, 2013.

Zhang, Y. M., Zhang, X. Y, Sun, J. Y.: Characterization of new particle and secondary aerosol formation during summertime in Beijing, China, Tellus, 63, 382–394, 2011.

Figure captions

Fig. 1 The (a) mass extinction coefficient, Kext (m^2 g), (b) SSA, and (c) ASY for six of the 12 model size bins for seven species of dry aerosols.

Fig. 2 The (a) mass extinction coefficient, Kext (m^2 g), (b) SSA, and (c) ASY of typical particle size (the red line in Fig. 1) for five hygroscopic aerosol species at six different rh.

Fig. 3 Monthly mean MODIS (topup) and modeled AOD (bottom) for July 2008.

Fig. 4 Daily variation of CRASNET observations (Obs.) and model-derived (Model) AOD from 1 to 31 July, 2008.

Fig. 5 Vertical distribution of atmospheric particle pollutants: (a) daily variations of 3JNS-the mean PM2.5 (μg m^{-3}) from 1 to 31 July, 2008; (b) the averaged extinction coefficient (K_{EXT}) (m^2 g^{-1}, left) and PM2.5 (right) for 7–11 July, 2008 for the 3JNS region.

Fig. 6 Daily changes of the 3JNS mean wind speeds (m s^{-1}) derived from the model and NCEP Reanalysis 2, together with simulated PM2.5 (μg m^{-3}) at 850–950 hPa (Fig. 6a) and at the surface (Fig 6b).

Fig. 7 Mean surface PM2.5 (μg m^{-3}, contour) and fktm (m^2 s^{-1}, shaded) for 7–11 July, 2008 (top) and the daily changes of the 3JNS mean PM2.5 and fktm for 1–31 July, 2008 (bottom).

Fig. 8 The mean surface PM2.5 (μg m^{-3}, contours) and PBL height (m, shaded) for 7–11 July, 2008 (top), and daily changes of the 3JNS mean surface PM2.5 and PBL height (bottom).

Fig. 9 Air pressure patterns (hPa, shaded), wind vectors at the surface (m s^{-1}, bottom), geopotential height (gph, shaded), wind vector at 950 hPa (middle) and 850 hPa (top) on 10 July (left) and 12 July, 2008 (right).

Table 1 Configured GRAPES_CUACE options for physical processes

Physical process	Configured options	References
Longwave radiation	Goddard	Chou et al., 2001
Shortwave radiation	Goddard	Chou et al., 1998
Cumulus clouds	KFETA Scheme	Kain, 2004
Surface Layer	SFCLAY Scheme	Pleim, 2007
Boundary layer	MRF Scheme	Hong and Pan, 1996
Land surface	SLAB Scheme	Kusaka et al., 2001
Cloud microphysics	KESSLER Scheme	Kessler, 1969
Gas-phase chemistry	RADM II	Stockwell et al., 1990
Aerosol chemistry	CUACE	Gong and Zhang, 2008

Table 2 CARSNET and AERONET station locations

Stations	Lat.	Long.	Altitude(m)
Beijing	39.80	116.47	31.3
Xianghe (AERONET)	39.76	117.00	
Datong	40.10	113.33	1067.2
Lanzhou	36.05	103.88	1517.2
SOCAL (AERONET)	35.57	104.08	
Shangdianzi	40.65	117.12	293.3
Longfengshan	44.73	127.60	330.5
Gucheng	39.13	115.80	15.1

Table 3 Observed and Modeled SSA, ASY and Model Bias

Station	Parameters	Obs.(times)	Model	Model Bias
Xianghe	SSA	0.96(10)	0.93	−3%
	ASY	0.74(10)	0.78	5%
SOCAL	SSA	0.95 (7)	0.90	−5%
	ASY	0.72(17)	0.77	7%

Fig. 1 The (a) mass extinction coefficient, K_{ext} (m^2 g), (b) SSA, and (c) ASY for six of the 12 model size bins for seven species of dry aerosols.

(a)

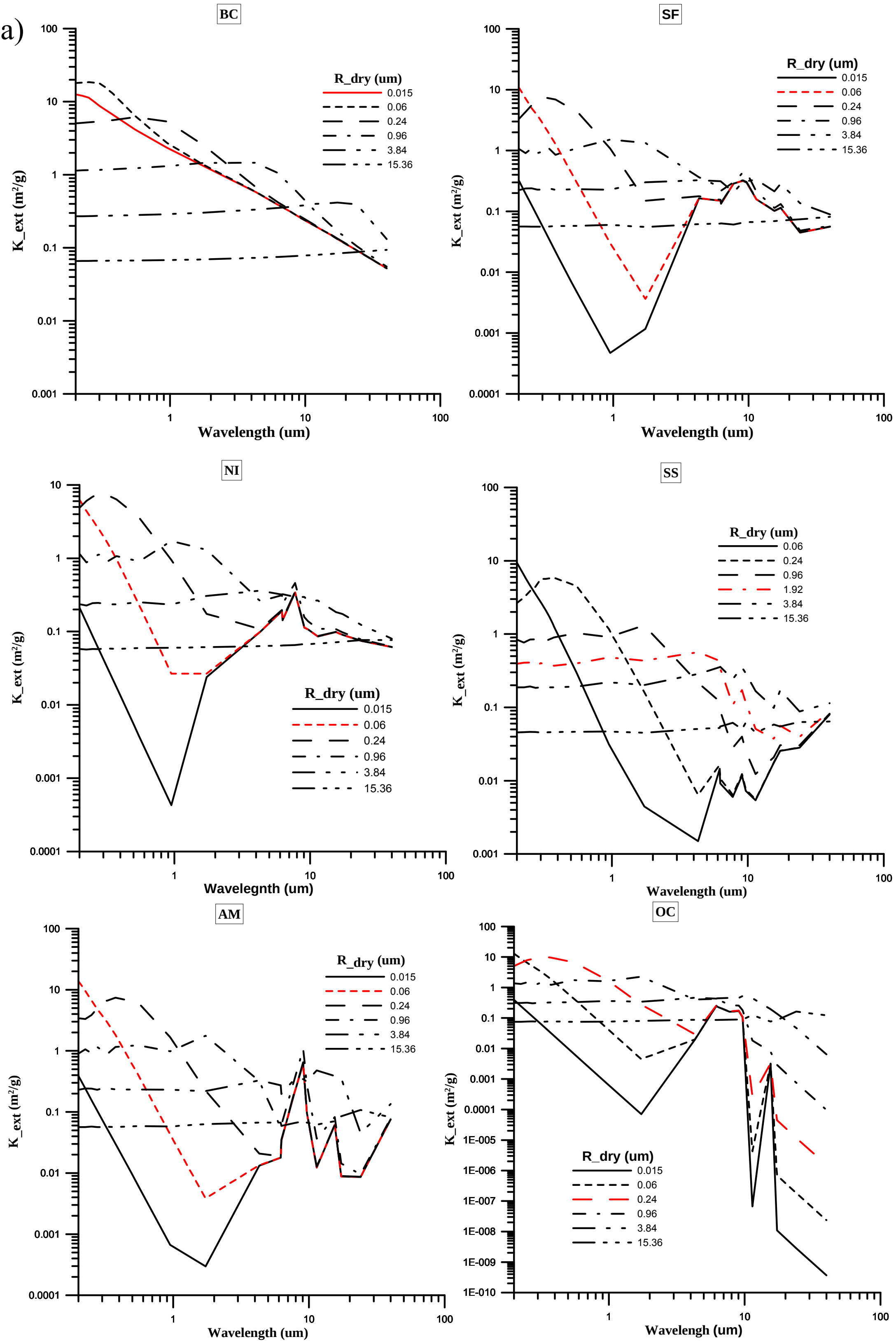

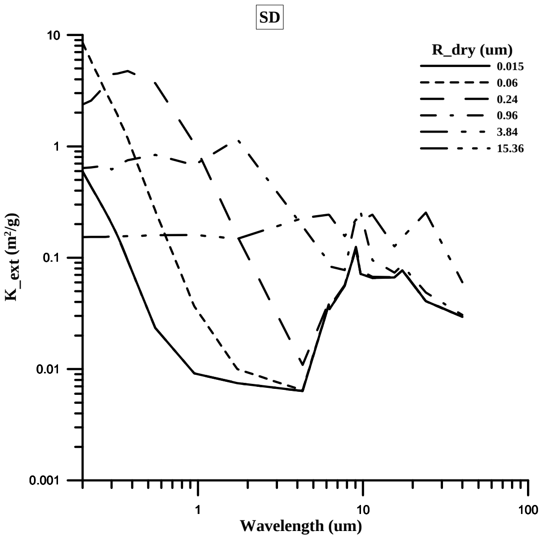
SD
R_dry (um)
0.015
0.06
0.24
0.96
3.84
15.36
K_ext (m²/g)
10
1
0.1
0.01
0.001
1
10
100
Wavelength (um)

(b)

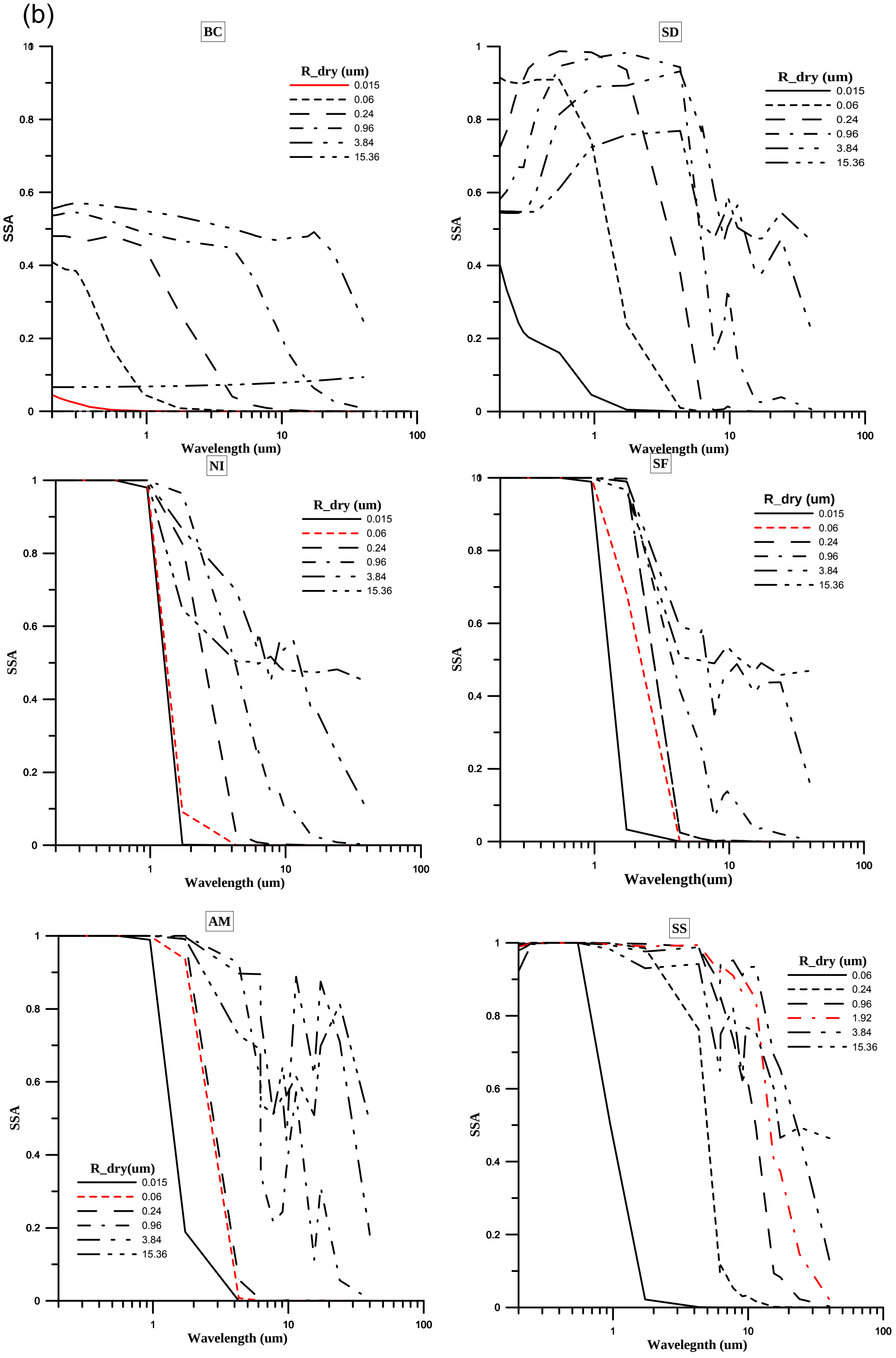
BC
R_dry (um)
0.015
0.06
0.24
0.96
3.84
15.36
SSA
Wavelength (um)
0
0.2
0.4
0.6
0.8
1
10
100
SD
R_dry (um)
0.015
0.06
0.24
0.96
3.84
15.36
SSA
Wavelength (um)
NI
R_dry (um)
0.015
0.06
0.24
0.96
3.84
15.36
SSA
Wavelength (um)
SF
R_dry (um)
0.015
0.06
0.24
0.96
3.84
15.36
SSA
Wavelength(um)
AM
R_dry(um)
0.015
0.06
0.24
0.96
3.84
15.36
SSA
Wavelength (um)
SS
R_dry (um)
0.06
0.24
0.96
1.92
3.84
15.36
SSA
Wavelegnth (um)

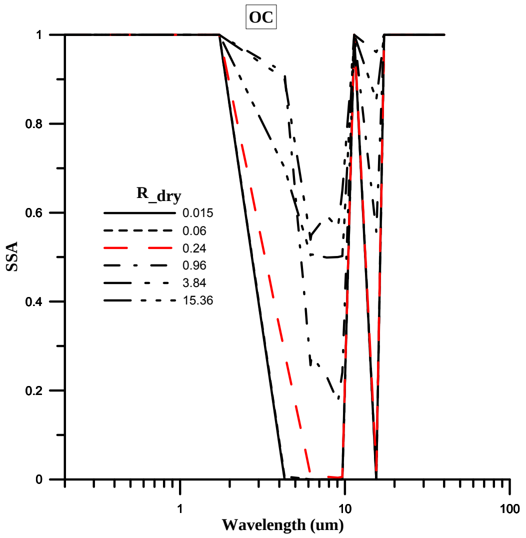
OC
SSA
1
0.8
0.6
0.4
0.2
0
1
10
100
Wavelength (um)
R_dry
0.015
0.06
0.24
0.96
3.84
15.36

(c)

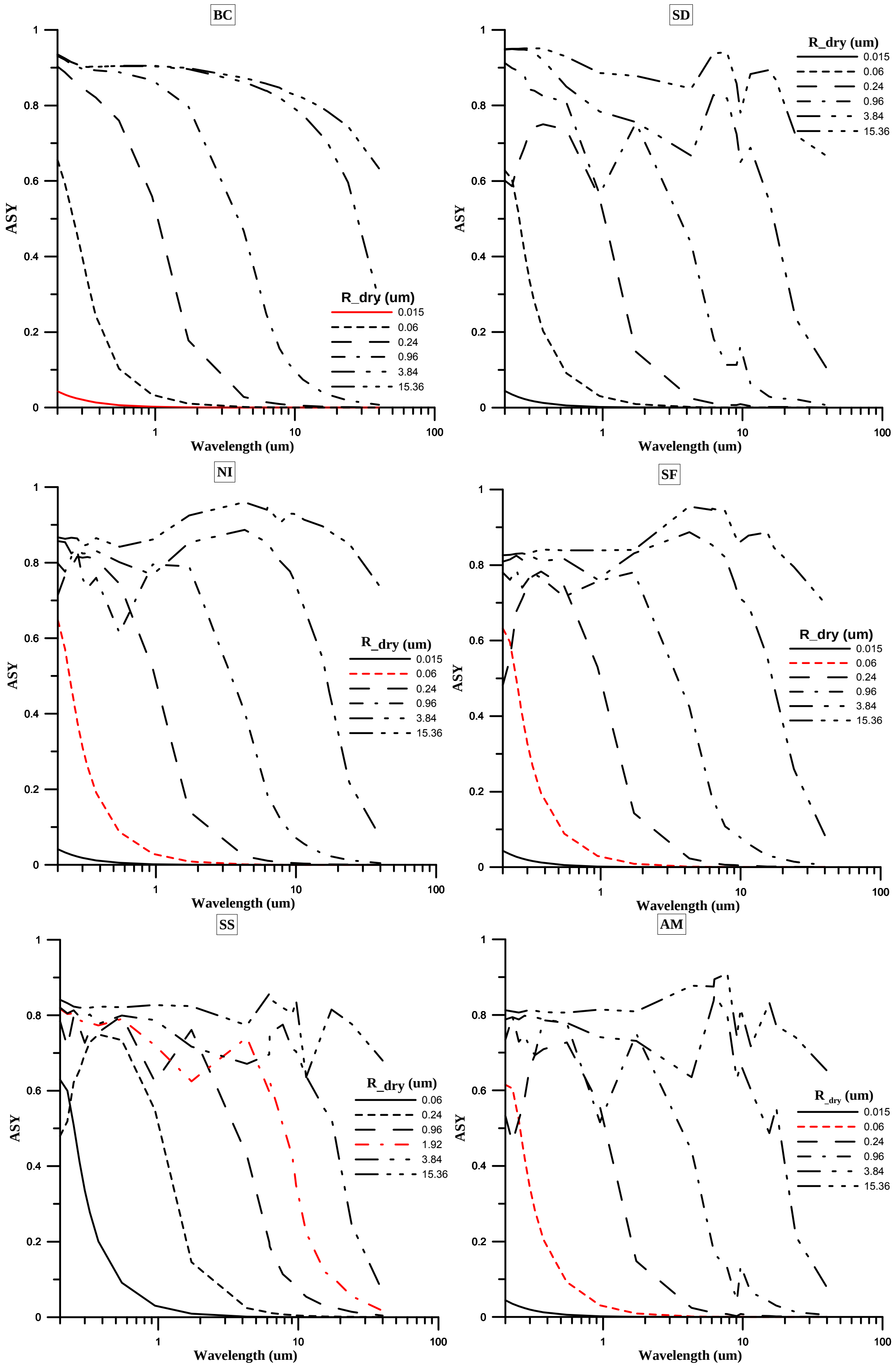
BC
SD
NI
SF
SS
AM
ASY
Wavelength (um)
0
0.2
0.4
0.6
0.8
1
1
10
100
R_dry (um)
0.015
0.06
0.24
0.96
1.92
3.84
15.36
R_dry (um)

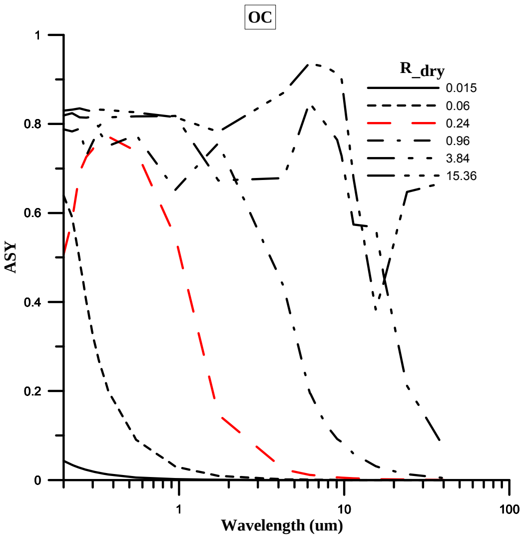
OC
R_dry
0.015
0.06
0.24
0.96
3.84
15.36
ASY
1
0.8
0.6
0.4
0.2
0
1
10
100
Wavelength (um)

Fig. 2 The (a) mass extinction coefficient, K_{ext} (m^2 g), (b) SSA, and (c) ASY of typical particle size (the red line in Fig. 1) for five hygroscopic aerosol species at six different *rh.*

(a)

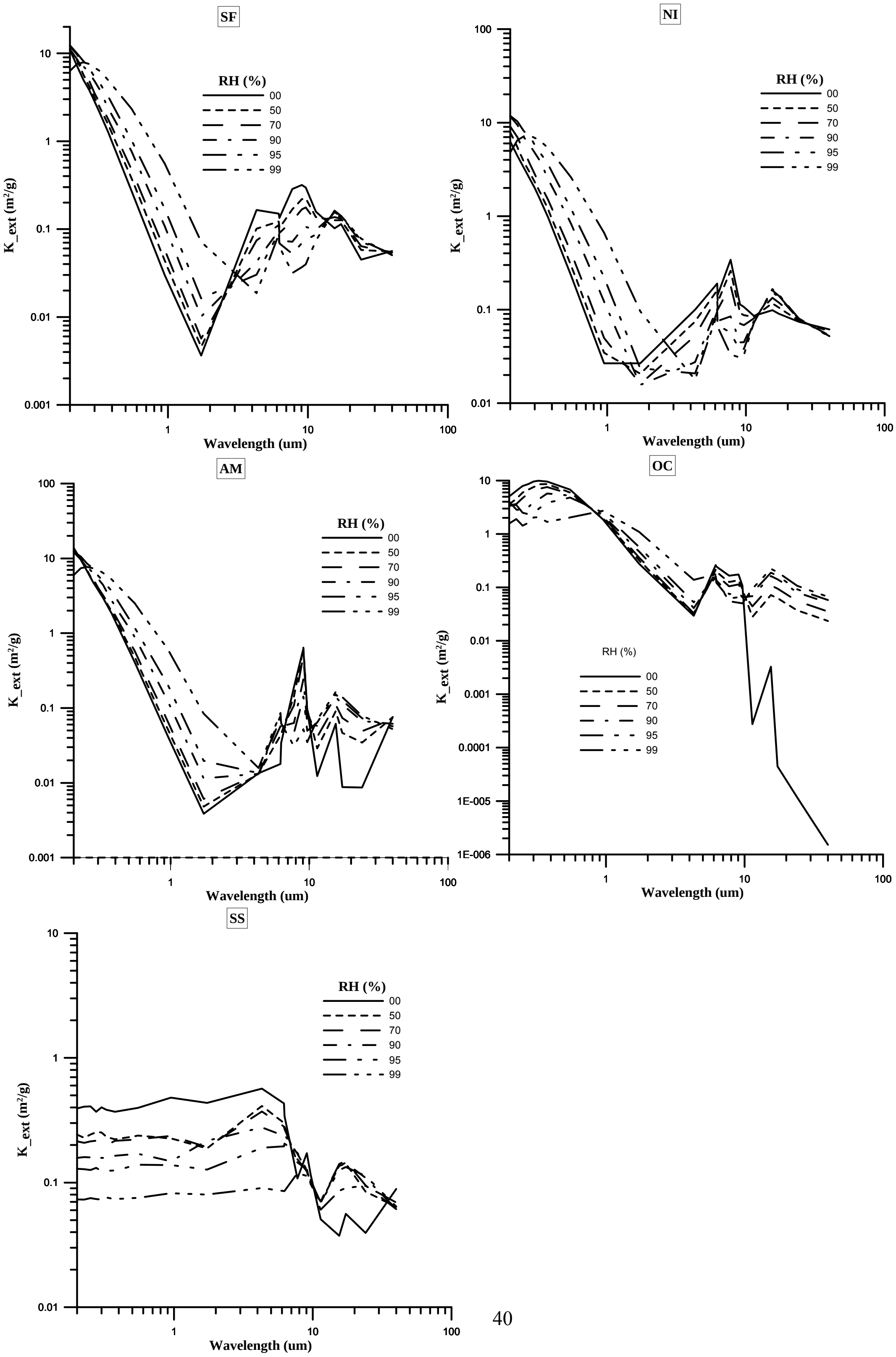

(b)

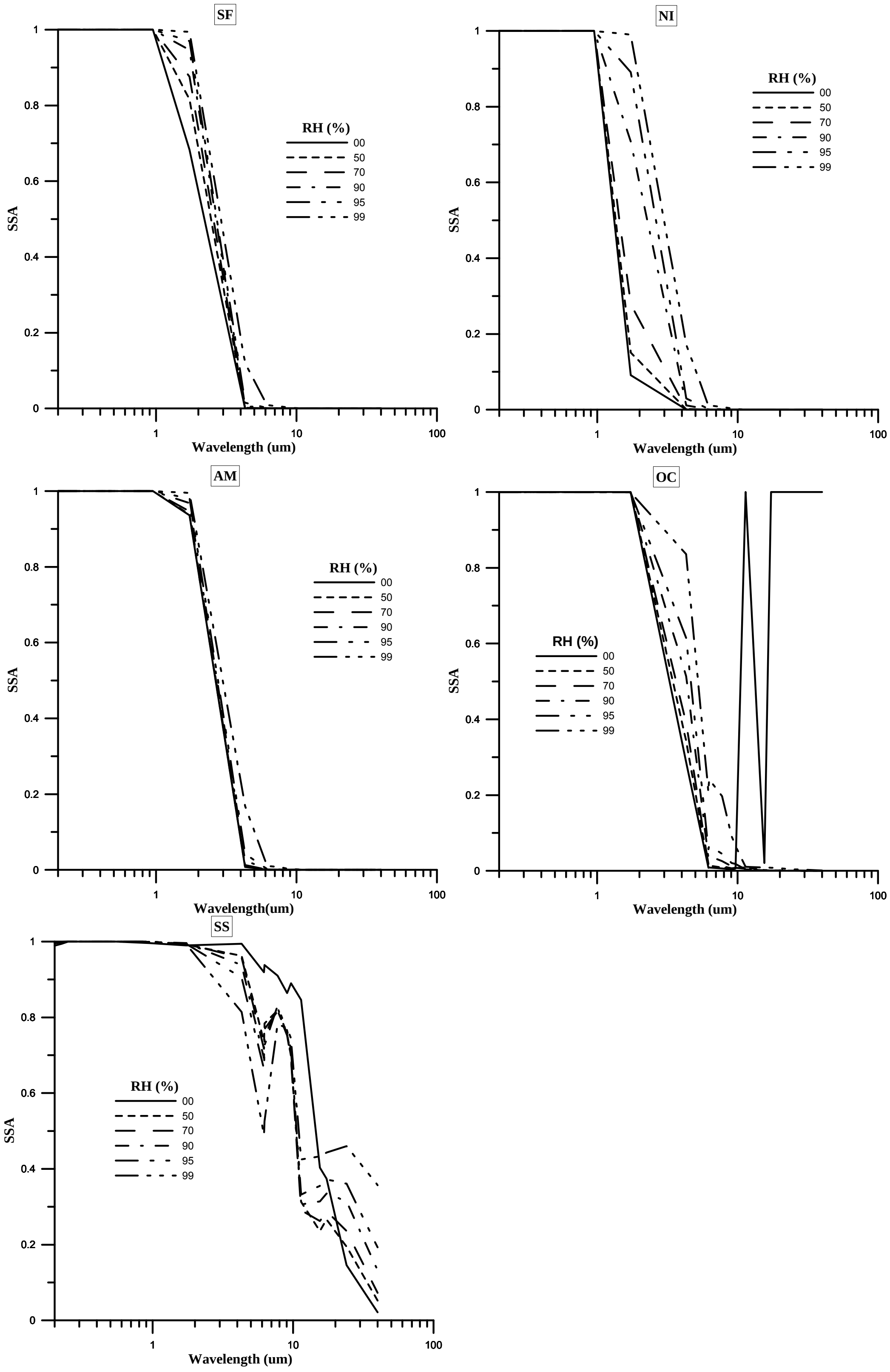
SF
NI
AM
OC
SS
SSA
Wavelength (um)
Wavelength(um)
RH (%)
00
50
70
90
95
99
0
0.2
0.4
0.6
0.8
1
1
10
100

(c)

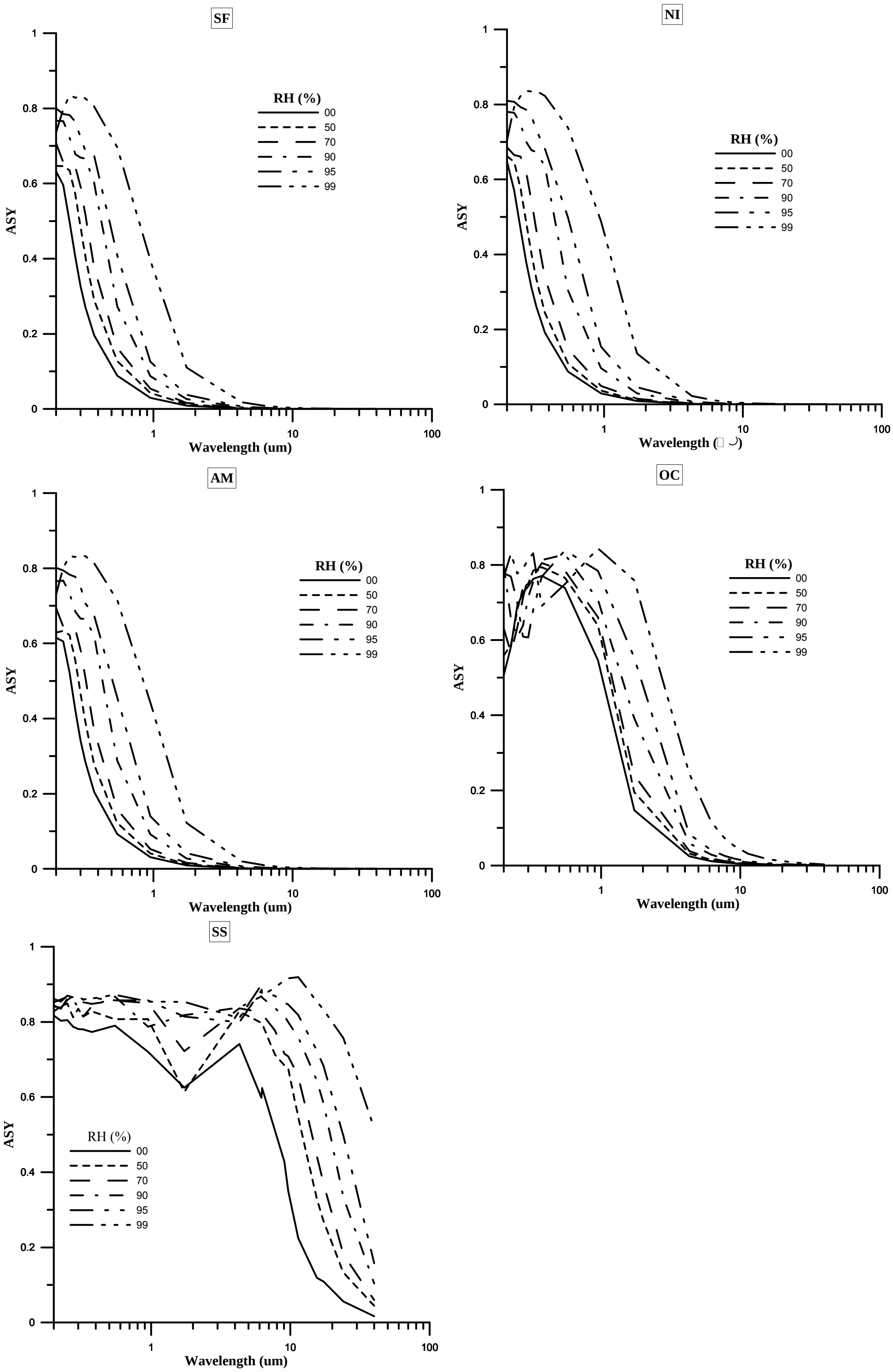
SF
NI
AM
OC
SS
ASY
Wavelength (um)
RH (%)
00
50
70
90
95
99
0
0.2
0.4
0.6
0.8
1
1
10
100

Fig. 3 Monthly mean MODIS (top) and modeled AOD (bottom) for July 2008.

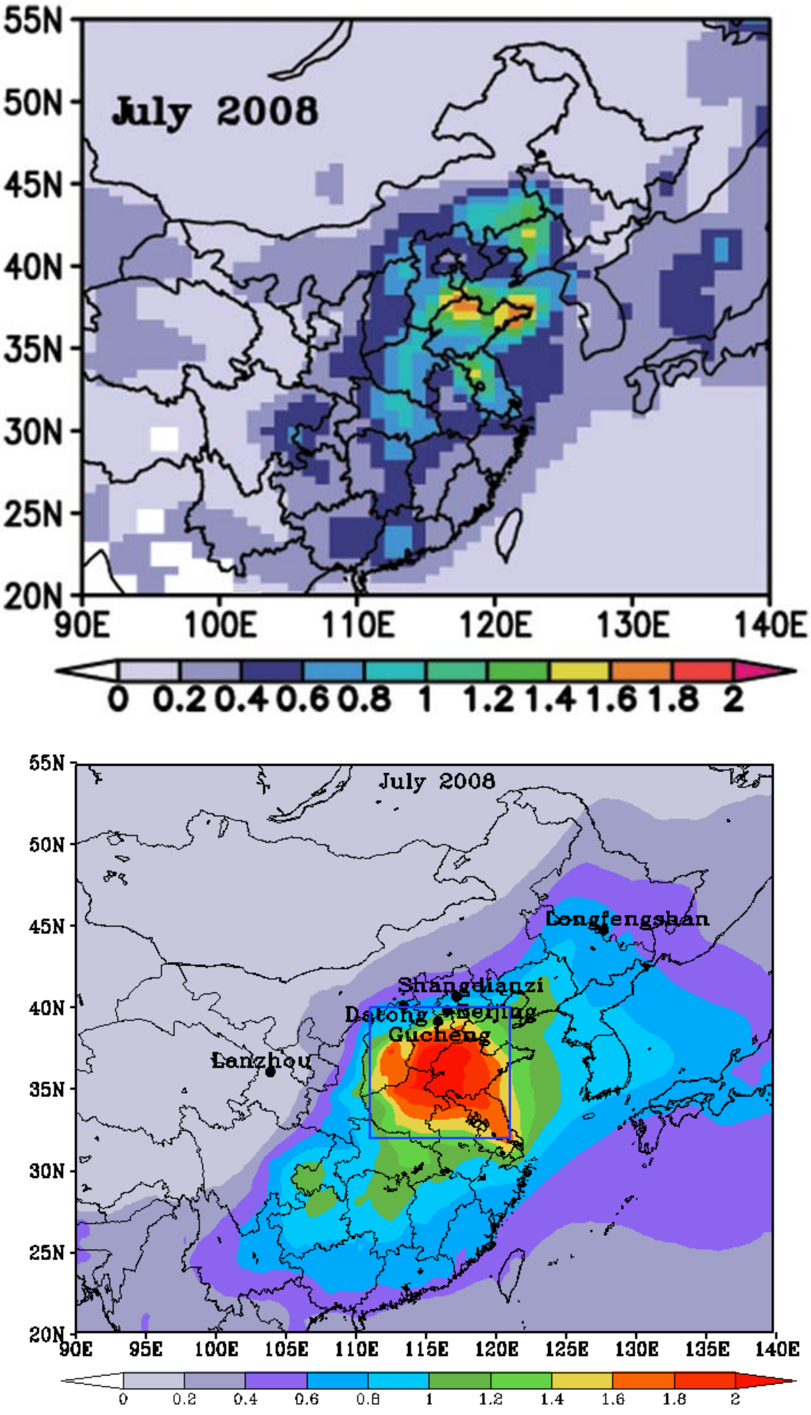

Fig. 4 Daily variation of CRASNET observations (Obs.) and model-derived (Model) AOD from 1 to 31 July, 2008.

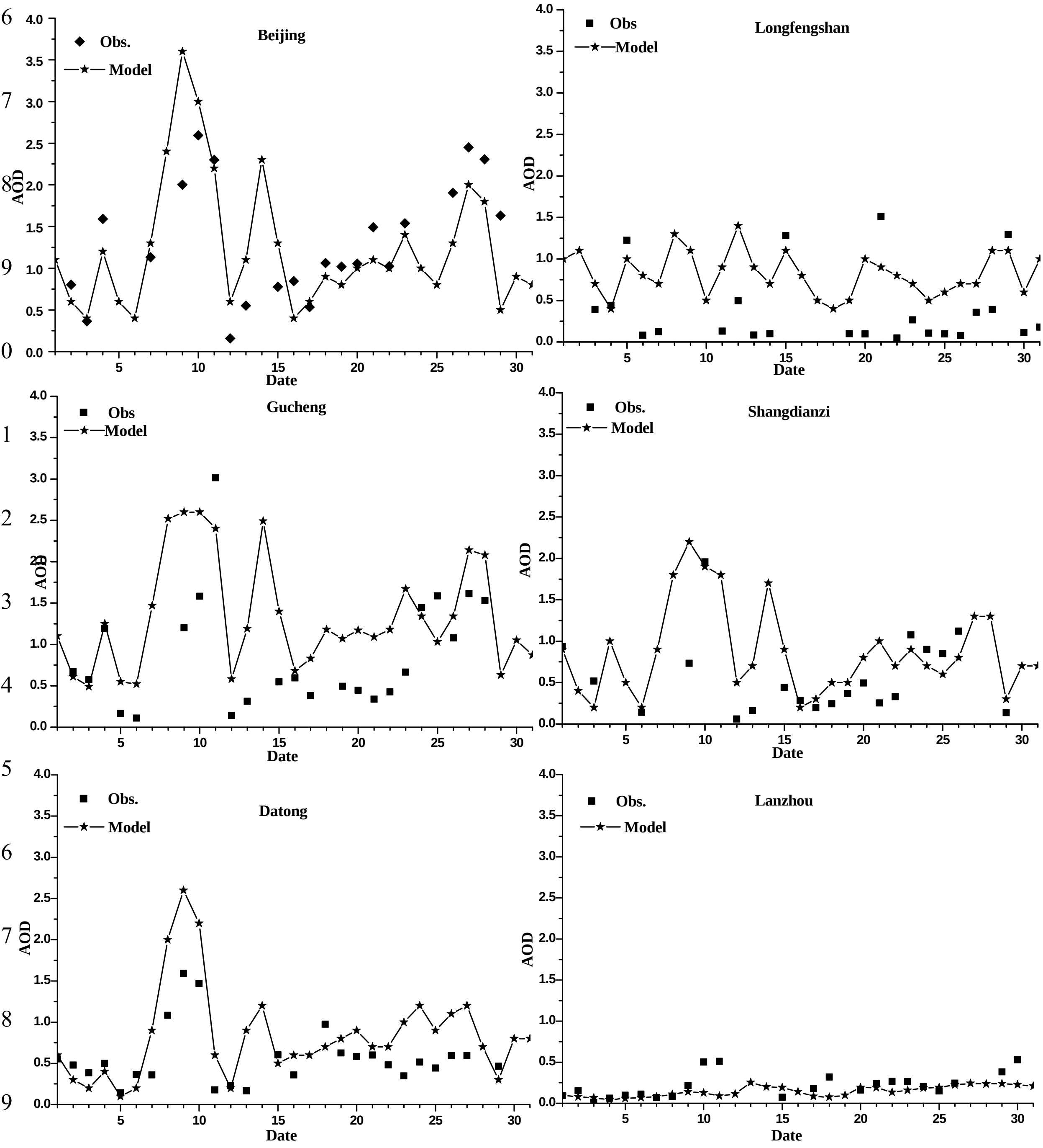

Fig. 5 Vertical distribution of atmospheric particle pollutants: (a) daily variations of 3JNS-the mean $PM_{2.5}$ ($\mu g\ m^{-3}$) from 1 to 31 July, 2008; (b) the averaged extinction coefficient (K_{EXT}) ($m^2\ g^{-1}$, left) and $PM_{2.5}$ (right) for 7–11 July, 2008 for the 3JNS region.

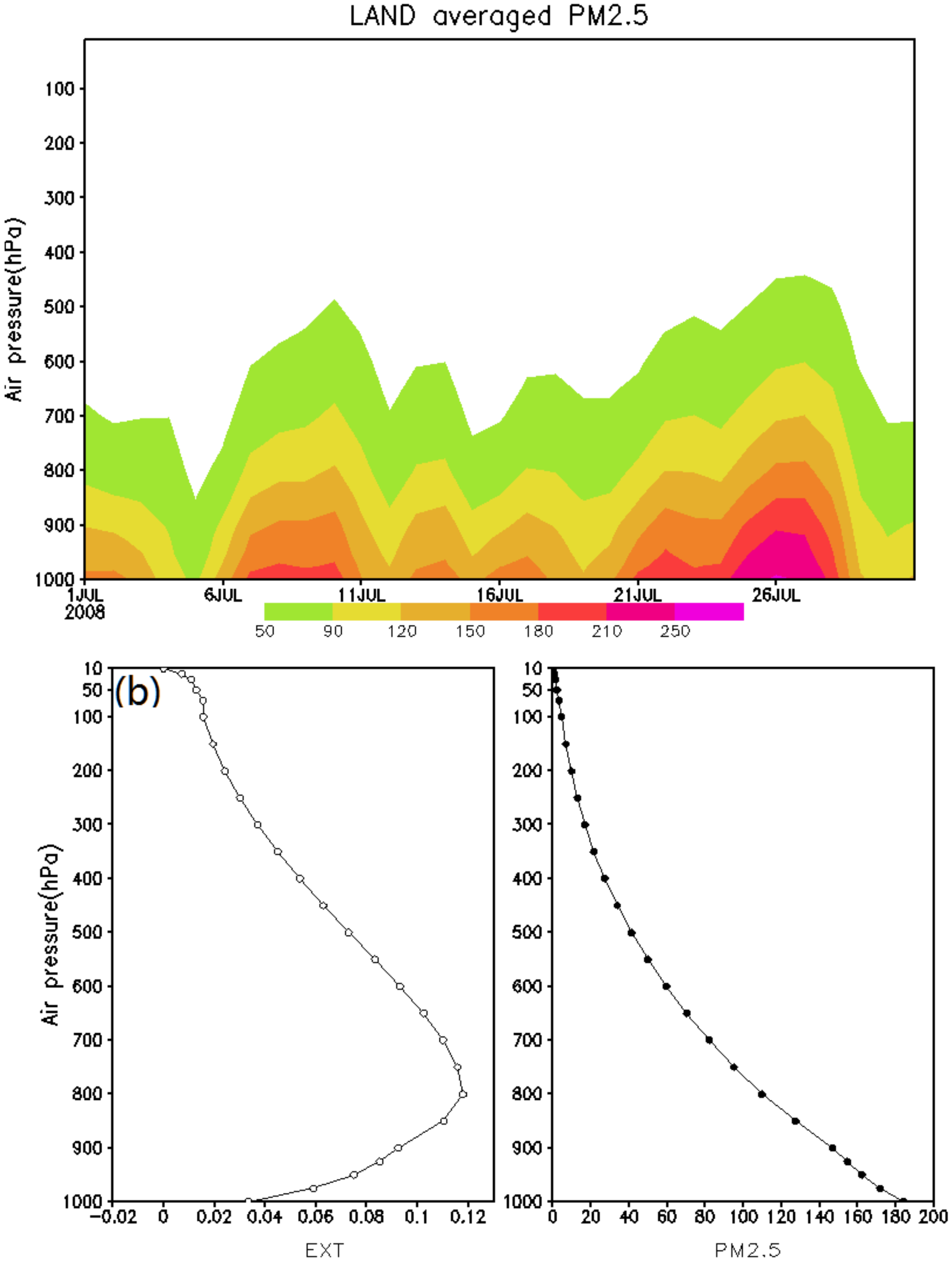

Fig. 6 Daily changes of the 3JNS mean wind speeds (m s^{-1}) derived from the model and NCEP Reanalysis 2, together with simulated $PM_{2.5}$ (μg m^{-3}) at 850–950 hPa (Fig. 6a) and at the surface (Fig 6b).

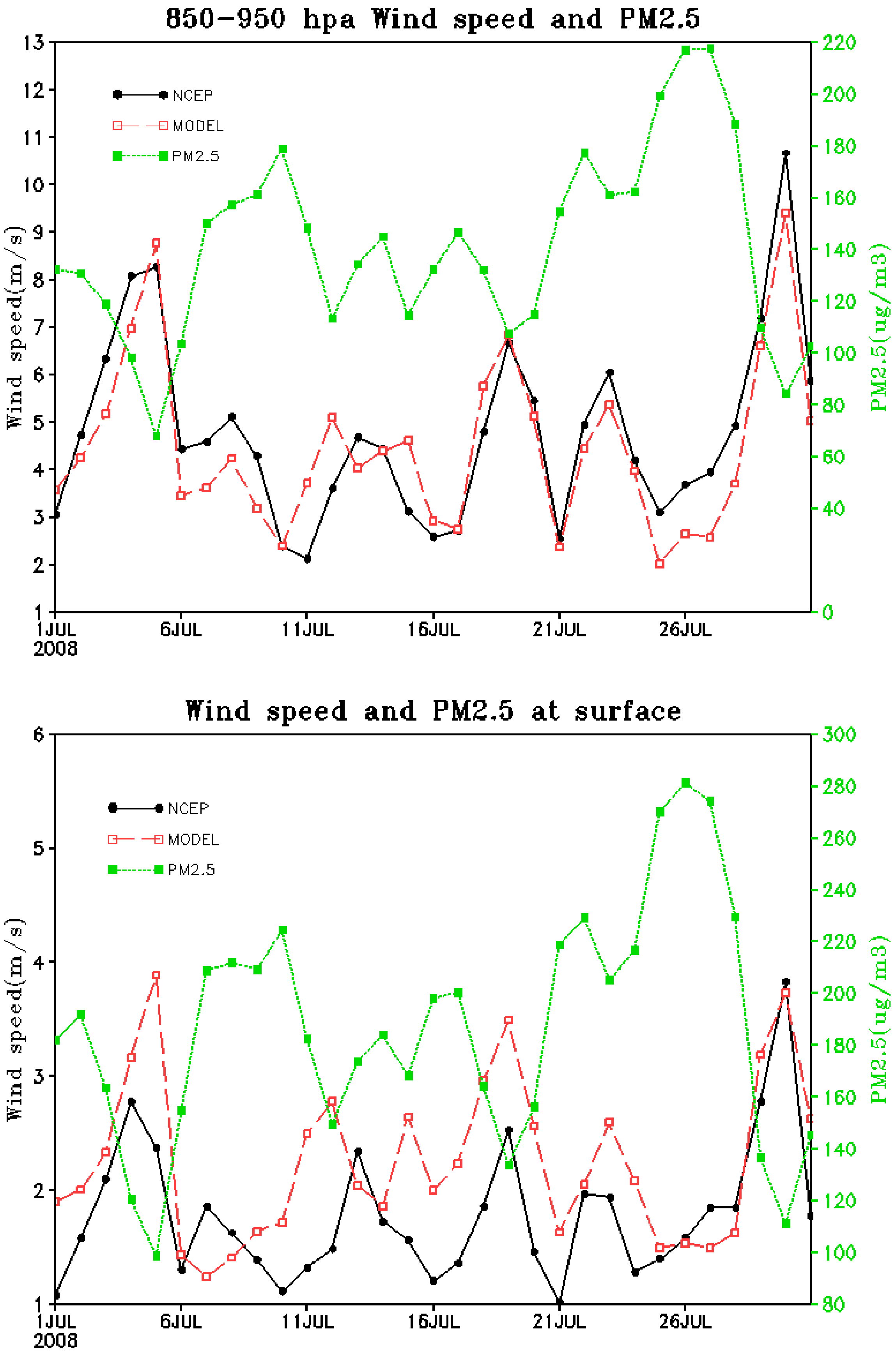

Fig. 7 Mean surface $PM_{2.5}$ ($\mu g\ m^{-3}$, contour) and f_{ktm} ($m^2\ s^{-1}$, shaded) for 7–11 July, 2008 (top) and the daily changes of the 3JNS mean $PM_{2.5}$ and f_{ktm} for 1–31 July, 2008 (bottom).

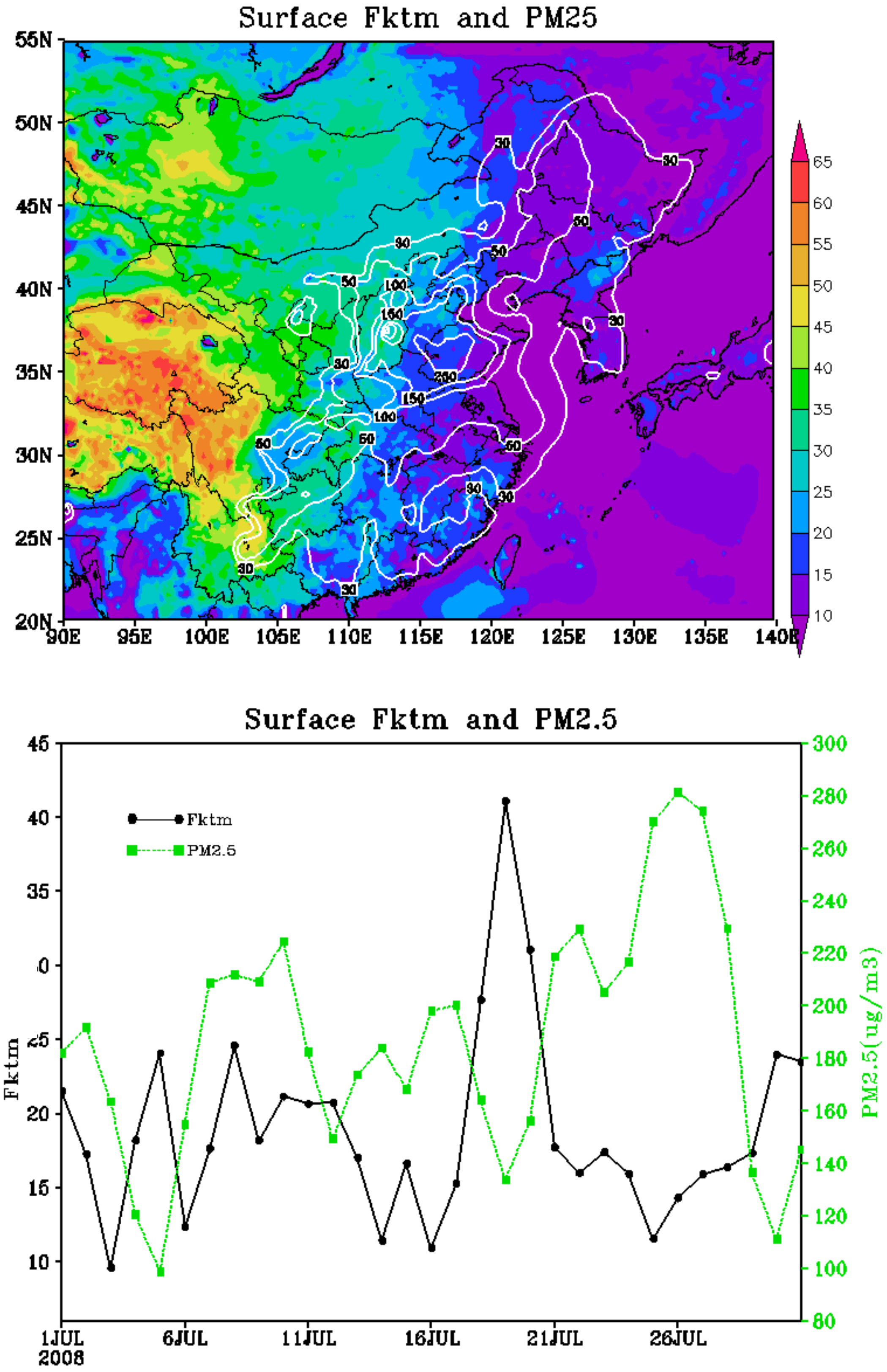

Fig. 8 The mean surface $PM_{2.5}$ ($\mu g\ m^{-3}$, contours) and PBL height (m, shaded) for 7–11 July, 2008 (top), and daily changes of the 3JNS mean surface $PM_{2.5}$ and PBL height (bottom).

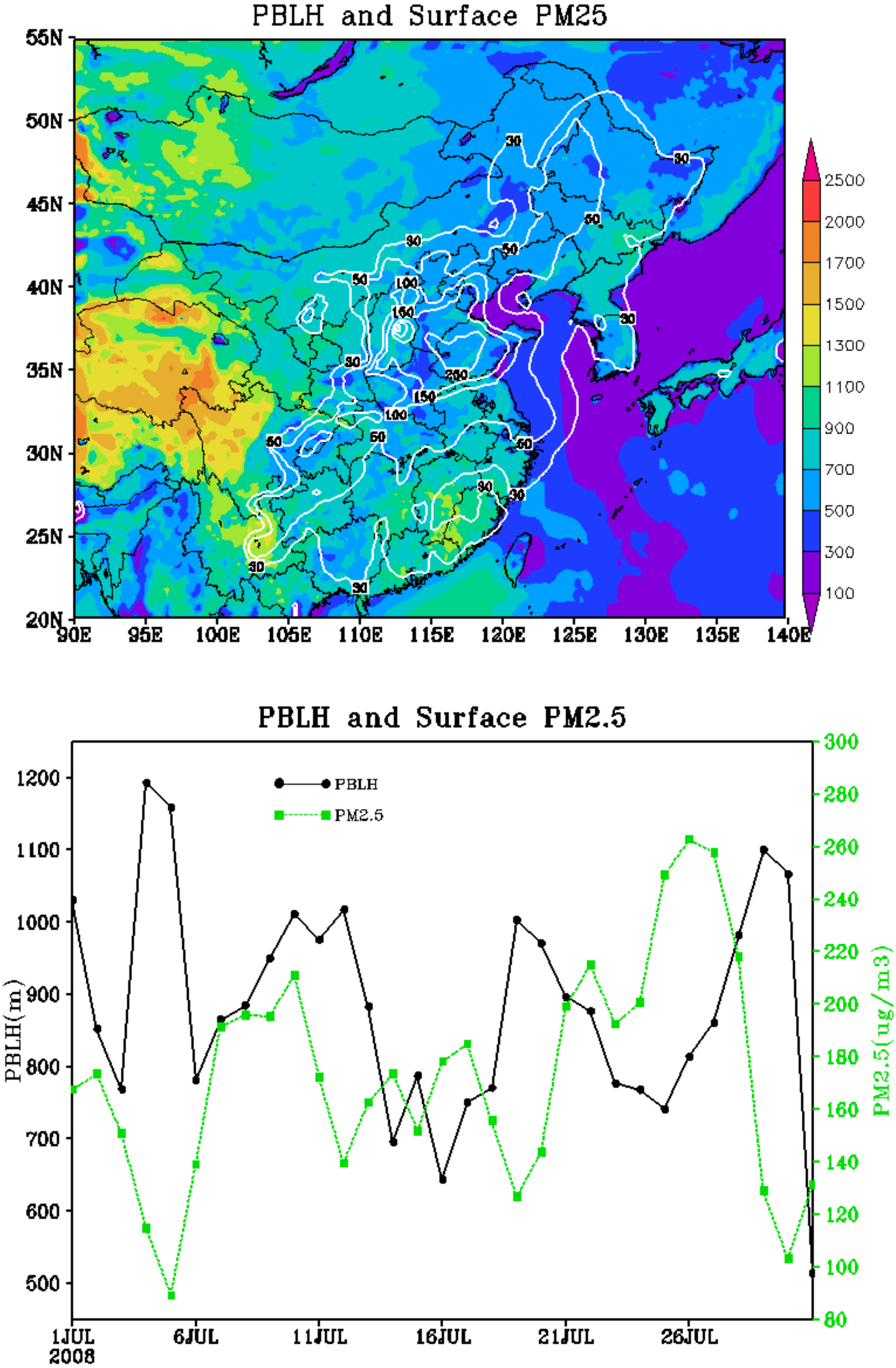

Fig. 9 Air pressure patterns (hPa, shaded), wind vectors at the surface (m s^{-1}, bottom), geopotential height (gph, shaded), wind vector at 950 hPa (middle) and 850 hPa (top) on 10 July (left) and 12 July, 2008 (right).